Frontiers of Physics
https://doi.org/10.1007/s11467-021-1047-z
Front. Phys.
16(4), 43300 (2021)

REVIEW ARTICLE

The origin of ultrasensitive SERS sensing beyond plasmonics

Leilei Lan, Yimeng Gao, Xingce Fan, Mingze Li, Qi Hao, Teng Qiu†

School of Physics, Southeast University, Nanjing 211189, China
Corresponding author. E-mail: †tqiu@seu.edu.cn
Received October 21, 2020; accepted December 27, 2020

Plasmon-free surface-enhanced Raman scattering (SERS) substrates have attracted tremendous attention for their abundant sources, excellent chemical stability, superior biocompatibility, good signal uniformity, and unique selectivity to target molecules. Recently, researchers have made great progress in fabricating novel plasmon-free SERS substrates and exploring new enhancement strategies to improve their sensitivity. This review summarizes the recent developments of plasmon-free SERS substrates and specially focuses on the enhancement mechanisms and strategies. Furthermore, the promising applications of plasmon-free SERS substrates in biomedical diagnosis, metal ions and organic pollutants sensing, chemical and biochemical reactions monitoring, and photoelectric characterization are introduced. Finally, current challenges and future research opportunities in plasmon-free SERS substrates are briefly discussed.

Keywords surface-enhanced Raman scattering, plasmon-free, enhancement mechanism, enhancement strategy, charge transfer

Contents

1 Introduction 1
2 The mechanisms of plasmon-free SERS 2
2.1 Mie resonance 2
2.2 Charge transfer resonance 3
2.3 Molecular resonance and exciton resonance 5
3 The strategies for improving the sensitivity of plasmon-free SERS 6
3.1 Defect engineering 6
3.2 Amorphization treatment 8
3.3 Phase engineering 10
3.4 Heterojunction engineering 11
3.5 Facet engineering 12
3.6 Molecular engineering 13
3.7 Other strategies 14
4 The applications of plasmon-free SERS 15
4.1 Biomedical diagnosis 15
4.2 Metal ions and organic pollutants sensing 16
4.3 Chemical and biochemical reactions monitoring 16
4.4 Photoelectric characterization 17
5 Summary and outlook 17
Acknowledgements 18
References 18

1 Introduction

As pioneers of surface-enhanced Raman scattering (SERS), Fleischmann *et al.* discovered the enhanced Raman scattering effect in 1974 [1], who initially attributed the signals increase to a higher number of adsorbed molecules with the increased surface area during measurements of the Raman scattering of pyridine on an electrochemically roughened silver electrode. This phenomenon was identified in 1977 by Jeanmaire & Van Duyne and Albrecht & Creighton independently [2, 3]. They both recognized that the tremendously strong surface Raman signals could not be explained by the increased surface area curtly and demonstrated the increased signals derived from a true enhancement of the Raman scattering efficiency itself, which created an exciting area of Raman spectroscopy, namely SERS. As one of the most powerful analytical tools, SERS overcomes the inherent shortcoming of weak signals in traditional Raman scattering with the magnification more than one million times. Besides, SERS requires less for the sample pretreatment and is more suitable for diverse analytical systems compared with mass spectrometry, fluorescence spectroscopy and other spectroscopy techniques. Over the past decades, tens of thousands research papers about SERS have been published, with SERS widely applied in various fields such as surface science, photonics, biomedicine, and trace analysis [4–10]. For example, the combination of scanning probe microscopy with SERS

*arXiv: 2101.06874. This article can also be found at http://journal.hep.com.cn/fop/EN/10.1007/s11467-021-1047-z.
Invited by Editor Shuai Dong.

has led to a new field, tip-enhanced Raman scattering (TERS), which provides abundant chemical signatures at high detection sensitivity up to single molecule and high spatial resolution up to (sub)nanometer [11, 12]. By the shell-isolated nanoparticle-enhanced Raman spectroscopy (SHINERS) technique, Li *et al.* studied the *in-situ* electrochemical behavior of different molecules and catalytic reactions [13]. In addition, Gu *et al.* demonstrated a physical unclonable functions label fabricated by drop-casting aqueous gap-enhanced Raman tags, which provides a potential platform to realize unbreakable anticounterfeiting [14]. However, high SERS activity almost only appears in the plasmonic noble-metal materials (mainly Au and Ag), and largely relies on the density of electromagnetic "hot spots" on the rough surface, which extremely limits the selection of materials [15]. Besides, these designed structures are particularly vulnerable to the environmental interference, indicating inferior stability. Apart from that, there are some other drawbacks including high cost and poor biocompatibility [16].

Compared with traditional plasmonic-based SERS, plasmon-free SERS, as a new frontier, possesses some special features. Firstly, plasmon-free SERS materials have abundant sources, including transition metal oxides [16–22], transition metal dichalcogenides (TMDs) [23–30], perovskites [31, 32], graphene [33–38], boron nitride [39–41], metal organic frameworks (MOFs) [42–45], organic semiconductors [46, 47], black phosphorus [48, 49, 51], and transition metal carbides and nitrides (MXenes) [52–58], which enable multiple choices to realize Raman enhancement [59]. Secondly, plasmon-free SERS materials do not require well-designed "hot spots", thus showing good signal uniformity and excellent stability, which could adapt to different detection environments. Moreover, multifunctional plasmon-free SERS materials are widely used in photoelectric devices, energy conversion, energy storage, catalysis and so on, which further expand the application scope of SERS [59, 60]. In addition, most of plasmon-free SERS materials are of low price, superior biocompatibility and recyclability. Whereas, the inferior detection sensitivity impedes the practical applications of plasmon-free SERS. Fortunately, some recent studies have made remarkable progress in obtaining ultrasensitive plasmon-free SERS substrates [47, 59, 61–63]. For instance, Ling *et al.* reported that graphene can be used as SERS substrates with a limit of detection (LOD) of 10^{-8} M [33]. Demirel *et al.* demonstrated that organic semiconductors could realize noble metal-comparable SERS enhancement and sensitivity by molecular engineering [47]. Seo *et al.* obtained the ultrasensitive plasmon-free SERS substrate with femtomolar detection limit on a two-dimensional (2D) van der Waals heterostructure [61]. As we know, the huge enhancement effect in SERS originates from the interaction between the SERS-active materials and probe molecules, generally including electromagnetic mechanism (EM) and chemical mechanism (CM) [6, 62]. In comparison to the EM-dominated plasmonic materials, plasmon-free materials own diverse surface physical and chemical properties, leading to more complicated enhancement mechanism. In the past for a long time, it was generally recognized that CM associated with charge transfer (CT) played a major role in plasmon-free SERS, based on which the enhancement factor (EF) is usually lower than 10^3 [62]. Nevertheless, according to the recent reports, there emerged more and more novel plasmon-free SERS substrates and the record of EF was continually broken, making the CT insufficient to explain the mechanism completely. As a result, we have to rethink the intrinsic nature of plasmon-free SERS.

Recent years, a series of new enhancement strategies including defect engineering [17–19], amorphization treatment [64–66], phase engineering [25, 27], heterojunction engineering [61, 67, 68], facet engineering [69, 70], molecular engineering [46, 47], and so on, have been used to improve the sensitivity of plasmon-free SERS materials, providing cases for understanding its enhancement mechanisms. These ultrasensitive plasmon-free SERS substrates expand the applications of plasmon-free SERS into various fields, ranging from bioanalysis to photoelectric characterization.

This review focuses on the background, enhancement mechanisms, enhancement strategies, and applications of ultrasensitive SERS sensing beyond plasmonics. At first, we introduce the background of SERS and the advantages of plasmon-free SERS. Afterwards, we discuss the enhancement mechanisms of plasmon-free SERS materials, followed by some strategies for improving their SERS sensitivity. Moreover, the applications of plasmon-free SERS materials in the areas of biomedical diagnosis, metal ions and organic pollutants sensing, chemical and biochemical reactions monitoring, and photoelectric characterization are summarized. Finally, future trend of plasmon-free SERS is briefly discussed.

2 The mechanisms of plasmon-free SERS

In recent years, as the plasmon-free SERS flourishes, the researches on its enhancement mechanisms have made remarkable progress. Until now, plenty of studies indicate that plasmon-free SERS strongly rely on material size, surface defect, sample morphology, crystallinity, and crystal orientation [64–72]. Some associated phenomena including Mie resonance, CT resonance, exciton resonance and molecular resonance may play important roles solely or synergistically.

2.1 Mie resonance

Mie resonance, known as morphology-dependent resonance, can give rise to strong local electromagnetic field and promote the interaction between light and mat-

ter. Compared with localized surface plasmon resonance (LSPR) in metallic particles, Mie resonance typically exists in dielectric particles [73, 74]. The Mie scattering can cause Raman enhancement when the particle size is comparable to the wavelength of incident light. This situation can be identified by an important size parameter x (i.e., $2\pi r/\lambda$), where r is the radius of the spherical particle, and λ is the wavenumber of the incident light. The Mie regime is defined for $0.1 < x < 100$. The scattering efficiency is the ratio of the power of the scattered light to that of the incident light [75]. Particularly, near dielectric sphere surfaces, the amplitude of the near-field scattering can be much larger than that of the far-field scattering, leading to a local electromagnetic field enhancement. According to Mie theory, the near-field scattering efficiency Q_{NF} is defined to evaluate the ability of a spherical particle to convert incident electric-field intensity into electric near-field intensity, which can be presented as follow [75]:

$$Q_{\mathrm{NF}} = 2\sum_{n=1}^{\infty}\left\{|a_n|^2\left[(n+1)\left|h_{n-1}^{(2)}(x)\right|^2 + n\left|h_{n+1}^{(2)}(x)\right|^2\right] + (2n+1)\,|b_n|^2\left|h_n^{(2)}(x)\right|^2\right\}, \quad (1)$$

where $h_n^{(2)}$ is the second kind of Hankel function, a_n and b_n are the scattering coefficients, which can be expressed by using the complex Riccati–Bessel functions ψ and ζ [76]:

$$a_n = \frac{\psi_n'(mx)\,\psi_n(x) - m\psi_n(mx)\,\psi_n'(x)}{\psi_n'(mx)\,\zeta_n(x) - m\psi_n(mx)\,\zeta_n'(x)}, \quad (2)$$

$$b_n = \frac{m\psi_n'(mx)\,\psi_n(x) - \psi_n(mx)\,\psi_n'(x)}{m\psi_n'(mx)\,\zeta_n(x) - \psi_n(mx)\,\zeta_n'(x)}, \quad (3)$$

where $m = n + \mathrm{i}k$ is the complex refractive index, n is the real refractive index and k is extinction coefficient part of the complex refractive. It should be noted that the complex refractive index is a fundamental physical property of a material, determined by the wavelength of incident light. Consequently, for a specific material, the near-field scattering intensity mainly depends on the size of spherical particle and the wavelength of incident light. Relevant theoretical studies indicate that the EF is approximately proportional to the second power of Q_{NF} [77]. Thus, Mie resonance provides giant Raman enhancement for dielectrics that are not able to generate LSPR in the visible region.

As early as 1988, Hayashi *et al.* observed increased Raman scattering from copper phthalocyanine (CuPc) molecules adsorbed on GaP nanoparticles with different sizes and explained the Raman enhancement in plamon-free materials by Mie scattering theory for the first time [78]. Recently, some groups reported significantly enhanced Raman scattering on plasmon-free materials through morphology-design-induced Mie resonance. Without plasmonic enhancers, Alessandri *et al.* observed remarkable Raman scattering enhancement on TiO_2 shell-based spherical resonators, which can be explained by multiple light scattering through the spheres, high refractive index of the shell layer, and related geometrical factors [79]. Further, they also demonstrated that the Mie resonance could be generated in 2 μm-size SiO_2/ZrO_2 core/shell beads utilized as all-dielectric Raman enhancers [80]. Rodriguez *et al.* reported that nonspherical silicon nanoparticles could generate strong SERS signals, this obvious enhancement stems from huge evanescent electromagnetic fields associated with the Mie resonance [81]. Besides, a remarkable enhancement of Raman sensitivity was obtained on submicron-sized spherical ZnO superstructures by Ji *et al.* (Fig. 1), which was attributed to the synergistic effect of CT in ZnO nanocrystals and Mie resonance of the superstructures [77].

2.2 Charge transfer resonance

CT resonance was first used to explain CM enhancement in plasmonic metals as EM mechanism fails to deal with all the SERS phenomena. For example, although CO and N_2 have similar Raman cross section, the Raman EF of CO is 200 times higher than that of N_2 under identical experimental conditions, which is unreasonable according to EM mechanism [82]. Jensen *et al.* summarized three

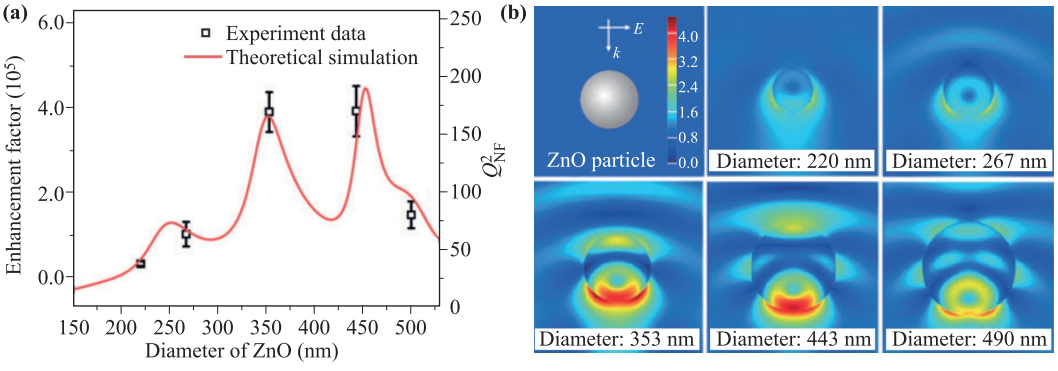

Fig. 1 **(a)** The EF and **(b)** electric near-field distribution of the ZnO particles with different diameters at a 532 nm excitation. Reproduced with permission from Ref. [77], Copyright © 2019 Wiley-VCH.

different situations where the SERS signals are enhanced due to the CM enhancement: (i) enhancement due to ground state chemical interactions between the molecule and nanoparticle which are not associated with the excitation wavelength of the SERS system, (ii) resonance Raman enhancement with the excitation wavelength resonant with a molecular transition, and (iii) CT resonance Raman enhancement when the excitation wavelength is resonant with the molecule-nanoparticle CT transitions [83]. Among these situations, ground state chemical enhancement is also referred to as the static chemical enhancement or non-resonance chemical enhancement, which is independent of the excitation wavelength because the Raman scattering process itself proceeds in a conventional fashion through virtual energy levels. However, it could also generate 10^0–10^2 Raman signal enhancements by the distortion and modification of the molecular electronic and skeleton structures. In order to explain the effect of resonance effect on Raman spectroscopy, fundamental quantum theorem of the Raman process is considered, in which the Raman process is expressed as a second order perturbation, including twofold interactions between molecules and light. The general expression for Raman polarization tensor $\alpha_{\sigma\rho}$ can be written by the Kramers–Heisenberg–Dirac dispersion formula [84, 85]:

$$(a_{\sigma\rho})_{if} = \sum_{n\neq i,f}\left[\frac{\langle i|M_\sigma|n\rangle\langle n|M_\rho|f\rangle}{E_n - E_i - \hbar\omega_0 - \mathrm{i}\Gamma_n} + \frac{\langle i|M_\rho|n\rangle\langle n|M_\sigma|f\rangle}{E_n - E_f + \hbar\omega_0 - \mathrm{i}\Gamma_n}\right], \quad (4)$$

where σ and ρ are the scattered and incident polarization directions, respectively; $|i\rangle$, $|n\rangle$ and $|f\rangle$ are the wavefunctions of the initial state, the intermediate state, and the final state of the molecular systems, respectively; E_i, E_n, and E_f are the energies of these states; M_σ and M_ρ are the electronic dipole moments in the directions of the Raman excitation and Raman scattering, respectively; $\hbar\omega_0$ is the energy of the excitation photon; Γ_n is the inverse of the dephasing time of the intermediate state. The first term $\frac{\langle i|M_\sigma|n\rangle\langle n|M_\rho|f\rangle}{E_n-E_i-\hbar\omega_0-\mathrm{i}\Gamma_n}$ can correspond to a resonance because the value of $E_n - E_f - \hbar\omega_0$ can be zero; the second term $\frac{\langle i|M_\rho|n\rangle\langle n|M_\sigma|f\rangle}{E_n-E_f+\hbar\omega_0-\mathrm{i}\Gamma_n}$ cannot represent a resonance, which is customarily neglected in a Raman process. Thus, the Raman resonance depends on the photon excitations of the molecule-metal system. Three different situations, including off-resonance ($E_n - E_f \gg \hbar\omega_0$), pre-resonance ($E_n - E_f \sim\hbar\omega_0$), and rigorous-resonance ($E_n - E_f = \hbar\omega_0$) should be considered in Raman resonance. Generally, Γ_n is in the order of 100 cm^{-1}, $E_n - E_f - \hbar\omega_0 >$10 000 cm^{-1} for off-resonance Raman scattering, and $E_n - E_f - \hbar\omega_0$ is about 0 cm^{-1} under the pre-resonance and rigorous-resonance. Therefore, the value of $\alpha_{\sigma\rho}$ for pre-resonance and rigorous-resonance is ~10^2 times larger than the off-resonance. The Raman intensity is in proportion to the square of the $\alpha_{\sigma\rho}$. So, a resonance Raman intensity is ~10^4 times larger than off-resonance Raman intensity [86]. Resonance effect in CM enchantment can be divided into two main types: (i) classical resonance effect of Raman scattering, namely, molecular resonance and (ii) the spectral changes caused by the CT processes in the molecule-substrate system, namely, CT resonance. Initially, CT resonance was proposed by Gersten and Burstein, respectively [87, 88]. While the direct evidence did not be given until 1981. In this year, Demuth *et al.* found the CT between the Fermi energy in metal and molecular energy levels by observing the excited electronic states in pyridine molecules [89]. Since 1980s, a series of SERS materials such as NiO [90], GaP [78] and TiO_2 [91] have been discovered and the CT resonance is therefore extended to the plasmon-free SERS materials. Taking semiconductor as an example, in the semiconductor-molecule system, the CT process would strongly depend on the efficiency of the vibronic coupling between the conduction band (CB) and valence band (VB) of semiconductors with the highest occupied molecular orbital (HOMO) and the lowest unoccupied molecular orbital (LUMO) of the adsorbed molecules. According to the thermodynamically permissible transitions in a semiconductor-molecule system, when the energy levels of semiconductors and molecules are matched well with each other, five possible CT pathways may occur, including molecule HOMO-to-CB, CT complex-to-CB, VB-to-molecule LUMO, surface state-to-molecule LUMO, and CB-to-molecule HOMO (Fig. 2) [62]. It should be noted that CT complex is formed by the strong chemical bonding between the molecule and semiconductor. Recently, many strategies have been reported to effectively increase the CT pathways in the system, leading to strong SERS effect [19, 31, 65, 67]. For example, by altering the wavelength of excited laser (473, 532, and 785 nm), Yu *et al.* found that a CT resonance could occur on the $MAPbCl_3$/4-Mpy interface when the excitation wavelength (532 nm) matches the band-band transition energy (2.32 eV) between $MAPbCl_3$ and 4-Mpy, which heightens the Raman signals of 4-Mpy molecule remarkably (EF = 2.6 $\times10^5$) [31]. Similarly, Yang *et al.* reported that the Ta_2O_5 substrate exhibits a remarkable SERS sensitivity with a low detection limit of 9 $\times10^{-9}$ M for methyl violet (MV) molecules by defect engineering [19]. In order to examine the interaction between Ta_2O_5 and the adsorbed MV molecule, the ultraviolet-visible absorption spectrum of MV-Ta_2O_5 complexes was collected to compare with those for neat MV and Ta_2O_5. The new broadened absorption peaks of the MV-Ta_2O_5 complexes were located in the range of 500–600 nm and indicated CT in this region, which was very close to the excitation wavelength (532 nm). Consequently, under irradiation with 532 nm, the substrate shows the strongest SERS activity with the quasi-resonance condition $\lambda_{CT} \approx \lambda_{laser}$ met. However, the Ta_2O_5 substrate presents poor SERS performance under two different excitation lasers (633 and 785 nm), which is most likely caused by the mismatch between the exci-

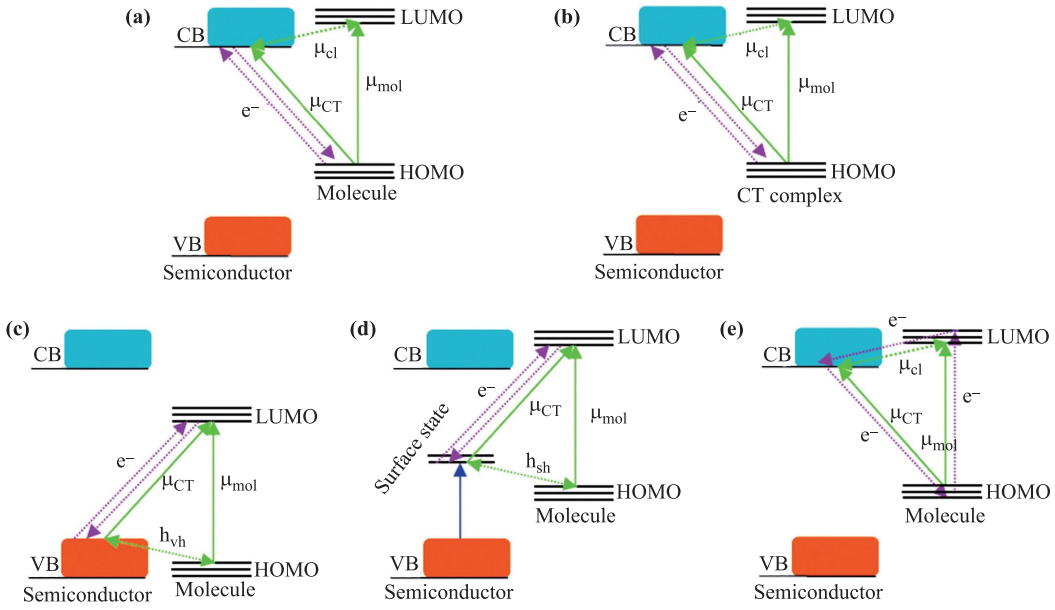

Fig. 2 The CT pathways in semiconductor-molecule systems **(a)** HOMO-to-CB, **(b)** CT complex-to-CB, **(c)** VB-to-molecule LUMO, **(d)** surface state-to-molecule LUMO, and **(e)** CB-to-molecule HOMO. Reproduced with permission from Ref. [62], Copyright © 2017 The Royal Society of Chemistry.

tation laser and the molecular and CT frequencies. In addition, some plasmon-free metallic materials also show ultrasensitive SERS sensing capacity, which involves in the CT process between the energy level of molecules and the Fermi level of metallic materials [25].

2.3 Molecular resonance and exciton resonance

The energy levels of molecules are divided into HOMO and LUMO. According to Albrecht and Lombardi' works [92–94], the $\alpha_{\sigma\rho}$ also can be expressed as $\alpha_{\sigma\rho}$ = A + B + C, where A term is relevant to the resonance Raman scattering, which follows the Franck–Condon selection rules and therefore only totally symmetric Raman modes are enhanced. The normal mode (Q_k) is determined by B or C term, which stems from the substrate-to-molecule and molecule-to-substrate CT transitions, respectively. Both totally and non-totally symmetric Raman modes can be enhanced by the B and C stems. And the resonance Raman scattering could be achieved when the laser excitation energy is close to the electronic transition energy of the molecule [59]. Further, according to the Herzberg-Teller coupling theory, the Raman scattering intensity contributed by the coupling of molecular resonance and charge transfer resonance is proportional to $|R_{mol-CT}(\omega)|^2$. Its expression can be described as [94]

$$R_{mol-CT}(\omega) = \frac{(\mu_{mol}\cdot E)(\mu_{CT}\cdot E)\, h_{mol-CT}\langle i|Q_k|f\rangle}{[(\omega_{Mie}^2-\omega^2)+\gamma_{Mie}^2][(\omega_{CT}^2-\omega^2)+\gamma_{CT}^2][(\omega_{mol}^2-\omega^2)+\gamma_{mol}^2]}, \tag{5}$$

where in Mie resonance ($\omega = \omega_{Mie}$) can be achieved by adjusting the size of particles. When $\omega = \omega_{CT}$ or $\omega = \omega_{mol}$, CT resonance or molecular resonance can be realized, respectively. The molecular resonance and CT resonance can be couple to each other through the Herzberg–Teller coupling constant (h_{ex-mol}). For instance, the resonances for rhodamine 6G (R6G) and MV molecules are both located in the visible region, which can well match with the wavelength of ordinary commercial lasers. Thus, R6G and MV have been widely exploited on the plasmon-free substrates to obtain ultrasensitive SERS sensing by coupling resonance [19, 64].

Exciton resonance is often ignored in the metal SERS field. However, in view of its crucial rule in semiconductor spectroscopy, the effect of excition resonance on semiconductor SERS spectrum should be considered. In the band structure of semiconductor, the VB and CB are separated by the band gap, similar to HOMO and LUMO of molecules. The electron can be excited from the VB to the CB under optical excitation and simultaneously a hole is created in the VB, thus forming an electron–hole pair. Electron and hole possess negative and positive charge respectively, so they are attracted to each other by coulomb forces. This strongly correlated electron–hole pair is called exciton and the exciton Bohr radius is considered as the distance in an electron–hole pair. The excition resonance

contributes to SERS in the same way as the molecular resonance, i.e., as a source of intensity borrowing. Thus, a new term involving the excition resonance in place of the molecular resonance can be described as [94]:

$$R_{ex-CT}(\omega) = \frac{(\mu_{ex} \cdot E)(\mu_{CT} \cdot E) h_{ex-CT} \langle i | Q_k | f \rangle}{((\omega_{Mie}^2 - \omega^2) + \gamma_{Mie}^2)((\omega_{CT}^2 - \omega^2) + \gamma_{CT}^2)((\omega_{ex}^2 - \omega^2) + \gamma_{ex}^2)}, \quad (6)$$

and the CT resonance or excition resonance can be realized when $\omega = \omega_{CT}$ or $\omega = \omega_{ex}$. They are couple to each other through the Herzberg–Teller coupling constant (h_{ex-CT}). For example, Lombardi *et al.* measured the SERS signals of 4-Mpy molecules absorbed on CdSe quantum dots (QDs) with different sizes, and a maximum EF as high as 10^5 was obtained in 5 nm CdSe QDs [95]. Further, they demonstrated that the exciton resonance plays a crucial role in Raman enhancement because the energy of incident light is close to exciton transition energy in 5 nm CdSe QDs. A vibrational coupling of the CT transition and exciton transition in CdSe-4-Mpy system leads to strongest SERS effect. Besides, our group fabricated a series of few-layer $MnPS_{3-x}$ Se_x ($0 \le x \le 3$). Among these 2D materials, the $MnPS_{2.4}Se_{0.6}$ shows the largest Raman enhancement with a LOD of 10^{-9} M because its exciton resonance at 2.20 eV is very close to the energy of incident light (2.32 eV). This result indicates that the synergistic resonances between CT and exciton resonance are crucial to the Raman enhancement in $MnPS_{2.4}Se_{0.6}$–R6G system (Fig. 3) [96].

3 The strategies for improving the sensitivity of plasmon-free SERS

In the past few decades, the inferior detection sensitivity impedes the practical applications of plasmon-free SERS. Fortunately, some recent studies have made remarkable progress in obtaining ultrasensitive plasmon-free SERS. A series of new strategies including defect engineering, molecular engineering, phase engineering, facet engineering, amorphization treatment, heterojunction, and morphology design have been used to improve the sensitivity of plasmon-free SERS, providing cases for understanding its enhancement mechanisms. It is distinct from the noble metals that several strategies can be applied simultaneously in plasmon-free SERS materials to further improve the SERS performance.

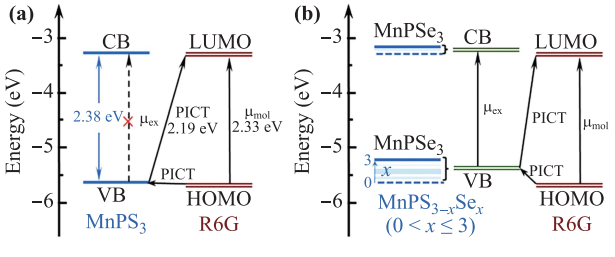

Fig. 3 Schematic illustration of the Raman enhancement mechanism for **(a)** $MnPS_{3-}$ and **(b)** $MnPS_{3-x}Se_x$ ($0 < x \le 3$)-R6G system. Reproduced with permission from Ref. [96], Copyright © 2020 Wiley-VCH.

3.1 Defect engineering

As a crucial research object in materials science, defect is closely related to many properties of material. Specifically, the crystal structure alters significantly when induced defects, such as forming vacancies or dislocations in the lattice, coinciding with changes in physical and chemical properties [97–99]. Based on this point, defect engineering has been extensively applied in catalysis, energy storage, photoelectric detection and so on [100, 101]. Recent years, by introducing defect engineering into SERS, researchers have realized the transformation from non-SERS activity to SERS activity successfully [17, 18, 24]. Thus, defect engineering has become an important strategy of adjusting plasmon-free SERS performance.

Served as one of the most widely studied SERS materials, the VB and CB of metal oxides are mainly contributed by the 2p orbital of oxygen and d orbital of metal atom respectively. Constructing defect in the metal oxides not only affects the position of VB, CB as well as the Fermi level, but also narrows the band gap through forming a defect energy level that provides an extra channel for the CT from the VB to the CB. The band structure changes are finally reflected in the absorption characteristics. Typically, the color of the tungsten oxide is turned from light yellow to purple or blue when oxygen vacancies inserted. It is worth noting that the band gap of metal oxides is generally higher than the excitation energy of Raman lasers, which seriously impedes the photo-induced charge transfer (PICT) between the metal oxide substrates and probe molecules, resulting in poor SRES performance. While the induced defects endow the metal oxides with narrower band gap and extra defect levels, thus broaden the CT access and facilitate PICT progress, which amplifies Raman scattering cross section significantly. Since the metal atoms in metal oxides are easily to be reduced with oxygen atoms missing in the crystal lattice, creating oxygen vacancies is the most common strategy for defect engineering. In this way, a series of high active SERS substrates including WO_{3-x} [17, 64], MoO_{3-x} [16, 102], TiO_{2-x} [103, 104], CrO_x [105], Cu_2O [18] and Ta_2O_5 [19] were reported. For

example, Zhao *et al.* prepared WO_{3-x} nanowires with the detection limit of R6G down to 10^{-7} M, comparable to some of noble metal SERS substrates [Figs. 4(a) and (b)] [17]. However, more defects do not mean higher SERS activities. By studying MoO_{3-x} with different oxygen vacancy concentrations, Wu *et al.* explored the relationship between the defect concentration and their SERS performance [102]. The Raman intensity mounts as the concentration increases initially. After reaching the maximum, the intensity dives until a stable value emerges. The mechanism behind this phenomenon is supposed that the different of CB, VB and Fermi level positions under different oxygen concentrations would change the relative position of molecular LUMO or HOMO levels towards MoO_{3-x}, ultimately resulting various SERS activities. Similar phenomenon has been observed on the TiO_2 SERS substrate doped with metal ions [106].

Apart from metal oxides, defect engineering could also regulate the SERS activity of the non-metal-oxide materials. Zhao *et al.* inserted oxygen atoms into the MoS_2 and obtained the narrower band gap and more electron states near the band edge. In consequence, the possibility of CT in the system would rise obviously under the illumination of laser, which further affects the CT between substrates and adsorbed molecules via vibration coupling. Compared to the samples without oxygen incorporation, the SERS activity of MoS_2 with proper oxygen incorporation is proven to be 10^5 times larger [(Figs. 4(c) and (d)] [24]. Besides, Zou *et al.* found the sulfur vacancies in monolayer MoS_2 would bring in extra electron states, which increases the EF up to 6.4 times [107]. By doping Ni into ZnS nanocrystals, the Raman intensity of 4-mercaptobenzoic acid (4-MBA) molecules detected on ZnS is magnified significantly [108]. Moreover, by controlling nitrogen doping, the Fermi level of graphene could be shifted and align with the LUMO of the molecule, significantly amplifying the vibrational Raman modes of the molecule. Thus, the nitrogen doped graphene showed an ultralow LOD of 10^{-11} M [34].

The technical approaches of creating defects in the SERS materials are roughly divided into two categories. On the one hand, we can adjust the synthesis procedure to produce defects directly. As a typical example, Guo *et al.* fabricated defective Cu_2O SERS substrates by the means

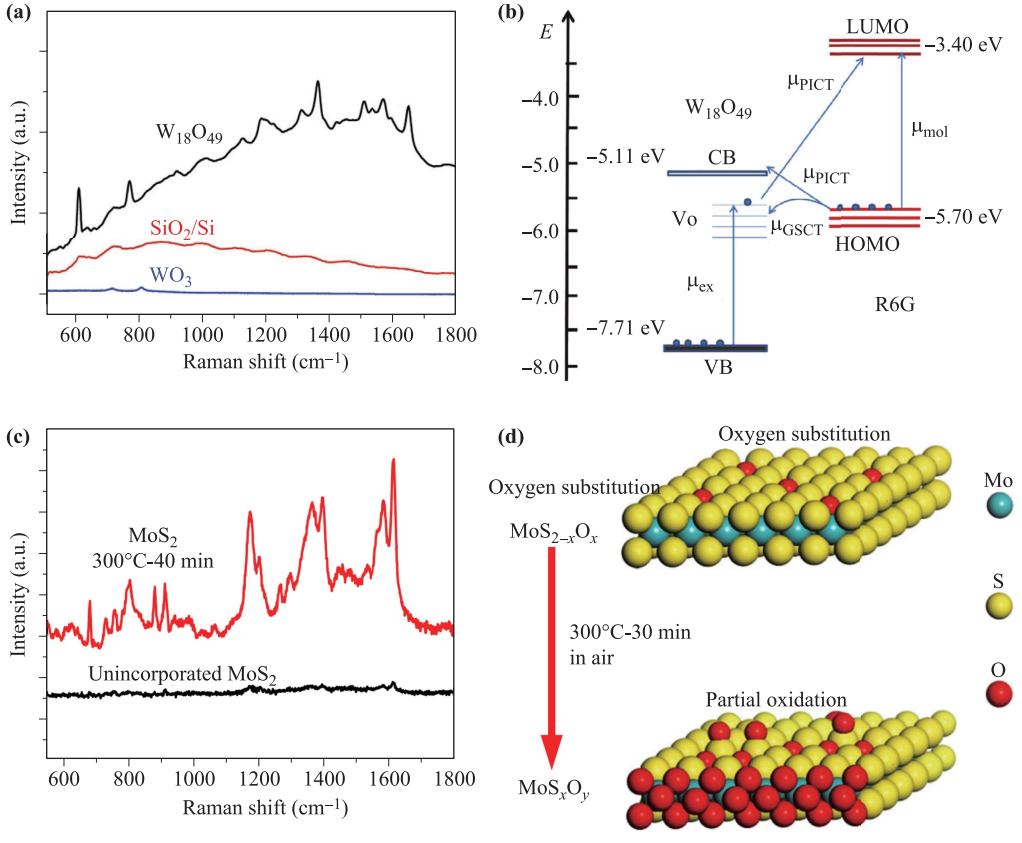

Fig. 4 Ultrasensitive SERS substrates are obtained by using defect engineering on $W_{18}O_{49}$ and MoS_xO_y. **(a)** SERS spectra of 10^{-6} M R6G adsorbed on $W_{18}O_{49}$, WO_3 and bare SiO_2/Si substrates. **(b)** Energy-level diagram of R6G on oxygen-deficit $W_{18}O_{49}$ measured in a vacuum. **(c)** SERS spectra of Victoria blue B on the partially oxidized MoS_2 sample at 300 °C for 40 min and unincorporated MoS_2. **(d)** Structure of oxygen-substituted and oxidized MoS_2. Reproduced with permission from (a and b) Ref. [17] and (c and d) Ref. [24], Copyright © 2015 and 2017 Springer Nature.

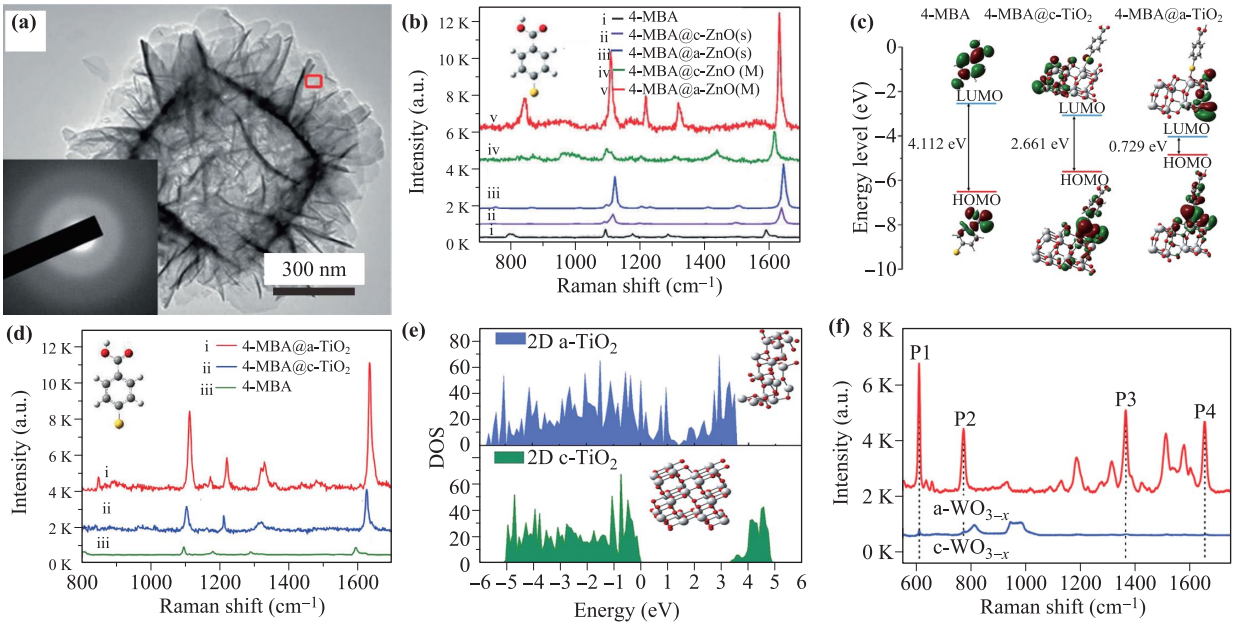

Fig. 5 Ultrasensitive SERS substrates are obtained by using amorphization treatment on ZnO, TiO_2 and WO_{3-x}. **(a)** SEM image of a-ZnO nanocages. **(b)** Measured (M) and simulated (S) SERS spectra of 4-MBA adsorbed onto a single a-ZnO nanocage. **(c)** Schematic energy level diagrams in the 4-MBA-TiO_2 system. **(d)** SERS spectra of 4-MBA adsorbed on a- and c-TiO_2 nanosheets. **(e)** DOS calculation of 2D a- and c-TiO_2. **(f)** SERS spectra of R6G adsorbed on a- and c-WO_{3-x} films. Reproduced with permission from (a and b) Ref. [65], (c)–(e) Ref. [66], and (f) Ref. [64], Copyright © 2017 Wiley-VCH, Copyright © 2019 American Chemical Society, Copyright © 2019 Wiley-VCH.

of chemical precipitation method, on which the LOD is as low as 10^{-9} M and the corresponding EF reaches 10^5 [18]. In our previous work, we fabricated MoO_{3-x} nanosheet ink by a solvothermal method and employed it to print the paper-based semiconducting SERS substrates successfully [16]. Yang *et al.* prepared Zn-doped TiO_2 nanoparticle SERS substrates by using a sol-hydrothermal method and explored the influence of Zn ions concentration on the SERS activity [109]. On the other hand, the secondary treatment for prefabricated materials could also accomplish defect engineering. The approaches general used include chemical reducing agent treatment, plasma processing, electrochemical reduction and so on [64, 110–112]. By reducing the WO_3 film via hydrogen gas, Fan *et al.* obtained the detection limit of R6G as low as 10^{-9} M [64]. And the limit of 5 $\times 10^{-8}$ M was realized on the metal oxide films irradiated with argon/nitrogen ion by Zheng *et al.* [110]. Through electrochemical reduction method, Cong and co-workers inserted metal ions into sputtered metal oxide films and prepared highly uniform SERS substrates with excellent performance [111].

In a word, as an effective strategy to improve SERS performance of plasmon-free materials, defect engineering breaks the limit of traditional noble metals and broadens the applications of plasmon-free compounds as SERS substrates. Table 1 shows the summary of the reported plasmon-free SERS substrates obtained by defect engineering in recent years.

3.2 Amorphization treatment

Although amorphous materials lack long-range atomic order, there still retain the basic building blocks and short-range order over a few atoms. For the crystal materials, electrons do not have absolutely free character due to their highly ordered periodic lattices. Nevertheless, the long-range unordered structure of the amorphous materials will produce the surface suspension bonds and band tails, which can promote the escape and transfer of surface electrons, and cause novel physical and chemical phenomena [145]. Recently, it has attracted increasing attention to introduce the amorphous materials into SERS researches [64–66]. For instance, Wang *et al.* designed a novel amorphous ZnO (a-ZnO) nanocage and the EF of mercapto molecules on these a-ZnO nanocages was up to 6.62 $\times 10^5$ [Figs. 5 (a) and (b)] [65]. First-principle density functional theory (DFT) calculation clearly confirmed that a-ZnO nanocages enabled more facile and efficient CT from the ZnO surface to the probe molecules compared to their crystalline counterparts. When mercapto molecules were adsorbed on the a-ZnO nanocages surface, the highly effective CT effect could even form the π bonding in the Zn-S bonds, which was further verified by the X-ray absorption near-edge structure (XANES) characterization. The metastable electronic states of a-ZnO nanocages surface impose a weaker constraint to the surface electrons, which could contribute to the efficient CT process in a-

Table 1 The summary of the reported plasmon-free SERS substrates obtained by defect engineering in recent years.

Substrate	Probe	LOD (M)	EF	Ref.
$W_{18}O_{49}$ nanowire	R6G	10^{-7}	3.4×10^5	[17]
WO_{3-x} film	R6G	10^{-9}	1.16×10^6	[64]
WO_{3-x} film	R6G	5×10^{-8}	1.1×10^4	[110]
Li_xWO_3 film	R6G	10^{-6}	8.86×10^4	[111]
$W_{18}O_{49}$ nanowire film	Rhodamine B (RhB)	10^{-7}	4.38×10^5	[113]
Mo doped Ta_2O_5 nanowire	MV	9×10^{-9}	2.2×10^7	[19]
Ta doped TiO_2 nanowire	Methylene blue (MB)	$< 2 \times 10^{-5}$	N/A	[114]
Ni doped TiO_2 photonic microarray	4-MBA	1×10^{-11}	3.3×10^4	[115]
Co doped TiO_2 nanoparticle	4-MBA	$< 10^{-3}$	N/A	[116]
Co doped TiO_2 nanoparticle	4-MBA	$< 10^{-3}$	N/A	[117]
Mn doped TiO_2 nanoparticle	4-MBA	$< 10^{-3}$	N/A	[106]
Zn doped TiO_2 nanoparticle	4-MBA	$< 10^{-3}$	N/A	[109]
C doped TiO_2 microparticle	4-MBA	$< 10^{-3}$	6.2×10^3	[118]
N doped TiO_2 nanofibre	4-MBA	$< 10^{-3}$	N/A	[119]
Black TiO_2 nanowire	R6G	1×10^{-7}	1.2×10^6	[103]
TiO_{2-x} QDs	Crystal violet (CV)	10^{-9}	$\sim 10^{10}$	[104]
TiO_2 nanoparticle	4-MBA	1×10^{-8}	N/A	[120]
CrO_x film	R6G	10^{-9}	N/A	[105]
MoO_{3-x} film	R6G	10^{-7}	N/A	[105]
MoO_{3-x} micron urchin	R6G	10^{-7}	$\sim 10^5$	[121]
MoO_{3-x} nanobelt	R6G	10^{-8}	1.8×10^7	[102]
MoO_{3-x} nanosheet	R6G	10^{-7}	3.32×10^5	[16]
V_2O_{5-x} nanoparticle	R6G	10^{-6}	N/A	[102]
V_2O_5 nanoparticle	R6G	10^{-8}	N/A	[122]
Nd doped ZnO nanoparticle	Malachite green	10^{-7}	N/A	[123]
Nd doped ZnO micron urchin	4-Mpy	N/A	N/A	[124]
Ga doped ZnO nanoparticle	4-MBA	$< 1 \times 10^{-3}$	8.13×10^3	[125]
Ni doped ZnO nanoparticle	4-MBA	$< 1 \times 10^{-3}$	N/A	[126]
Co doped ZnO nanoparticle	4-MBA	$< 1 \times 10^{-3}$	N/A	[127]
Mg doped ZnO nanocrystal	4-MBA	N/A	N/A	[128]
ZnO QDs	CV	10^{-9}	$\sim 10^6$	[129]
ZnO nanosheet	4-Mpy	1×10^{-7}	7.7×10^5	[130]
ZnO nanoparticle	Methyl orange	$< 1 \times 10^{-3}$	56	[131]
Cu_2O Superstructure particle	R6G	10^{-9}	8×10^5	[18]
SnO_2 nanoparticle	4-MBA	$<1 \times 10^{-3}$	3.4×10^3	[132]
O doped 2H-MoS_2 nanosheet	R6G	10^{-7}	1.4×10^5	[24]
O doped 1T-MoS_2 nanosheet	R6G	10^{-11}	1.24×10^7	[133]
O doped 2D-MoS_2	R6G	$< 10^{-5}$	N/A	[134]
MoS_{2-x} monolayer	R6G	$< 10^{-6}$	N/A	[107]
$Cu_{2-x}S$ nanoparticle	R6G	10^{-7}	3.4×10^4	[135]
Zn doped ZrO_2 nanoparticle	4-MBA	$< 1 \times 10^{-3}$	1.94×10^4	[136]
Indium tin oxide (ITO) film	R6G	$< 10^{-5}$	N/A	[137]
ITO film	R6G	1×10^{-7}	N/A	[138]
Ni doped ZnS nanoparticle	4-MBA	$< 1 \times 10^{-3}$	N/A	[108]
2D Sb:Na	R6G	10^{-16}	N/A	[139]
ZnSe nanowire	R6G	10^{-11}	6.12×10^7	[140]
N doped graphene	R6G	10^{-11}	N/A	[34]
N doped graphene QDs	RhB	10^{-10}	3.2×10^3	[37]
Fe-N-doped carbon nanosheet/rod	R6G	1×10^{-7}	3.8×10^4	[141]
B doped diamond film	MB	1×10^{-7}	3.2×10^5	[142]
Reduced $Ti_3C_2T_x$ nanosheet	R6G	1×10^{-7}	1.0×10^7	[52]
Reduced $MnCo_2O_4$ nanotube	CV	1×10^{-5}	1.34×10^6	[143]
S doped $SnSe_2$ nanosheet	R6G	1×10^{-7}	N/A	[144]
WSe_{2-x} monolayer	CuPc	N/A	120	[112]

ZnO-molecule system, leading to significant magnification of the molecular polarization and remarkable enhancement of Raman scattering. Furthermore, they fabricated novel 2D amorphous TiO_2 (a-TiO_2) nanosheets, which ex-

hibited a remarkable SERS sensitivity with an ultrahigh EF of 1.86 $\times 10^6$, stronger than that of their 2D crystalline TiO_2 (c-TiO_2) nanosheets counterparts [Figs. 5 (c)–(e)] [66]. According to the results of DFT calculations, the band gap of 4-MBA@a-TiO_2 complex was only 0.729 eV, smaller than that of the 4-MBA@c-TiO_2 complex (2.661 eV). As the HOMO-LUMO energy gap of 4-MBA was about 4.112 eV, the obviously reduced band gap of the 4-MBA@a-TiO_2 complex could be ascribed to the strong energy level coupling between the 4-MBA molecule and the 2D a-TiO_2, which allowed more possible thermodynamic PICT excitations at the low-energy level and hence effectively enhanced the Raman signals. Besides, DFT calculations and experimental results further revealed that the 2D a-TiO_2 nanosheets possessed smaller band gap and higher electronic density of states (DOS) than that of their crystal counterparts, which further effectively enhanced the vibronic coupling of resonances in the a-TiO_2-molecule system, resulting in a high-efficient PICT process. In addition, our group also observed ultrasensitive SERS activity in amorphous tungsten oxide (a-WO_{3-x}) films with a high EF of 1.16 $\times 10^6$ [64]. Compared with crystalline WO_{3-x} (c-WO_{3-x}) films, a-WO_{3-x} films exhibited narrower band gap, stronger exciton resonance, and higher DOS near the Fermi level, which could promote the PICT resonance between analytes and substrates by offering efficient routes of charge escaping and transferring as well as strong vibronic coupling, thus realizing ultrasensitive SERS activity on a-WO_{3-x} films [Fig. 5(f)]. Besides, researchers have also observed strong SERS signals from some amorphous materials, such as Rh_3S_6 [146], $M(OH)_x$ (M = Fe, Co, Ni and Zn) [147, 148], Nb_2O_5 [149]. However, for the future development of amorphous material-based SERS substrates, there are still some obstacles to be settled. For example, the present preparation process of amorphous SERS materials is pretty complicated thus a new convenient and controllable synthetic method is urgently needed. And it is still a challenge to optimize the energy band structure and surface physicochemical properties of amorphous SERS materials for the programmable control of CT pathways and coupling enhancement.

3.3 Phase engineering

TMDs possess complex and variable phase structures and electronic structures. Taking MoS_2 as an example, the steady phase is hexagonal structure (2H phase), belonging to semiconductor. While once the position of coordinating atoms in 2H-MoS_2 is induced to be altered, metastable octahedral structure is formed, which is called metallic 1T-MoS_2 [150]. Recently, metallic/semimetallic TMDs have attracted much attention due to their unique physical and chemical properties [151, 152]. More importantly, metallic/semimetallic TMDs possess large DOS near the Fermi levels and high surface activities, indicating that they can provide strong molecule-SERS substrate coupling as well

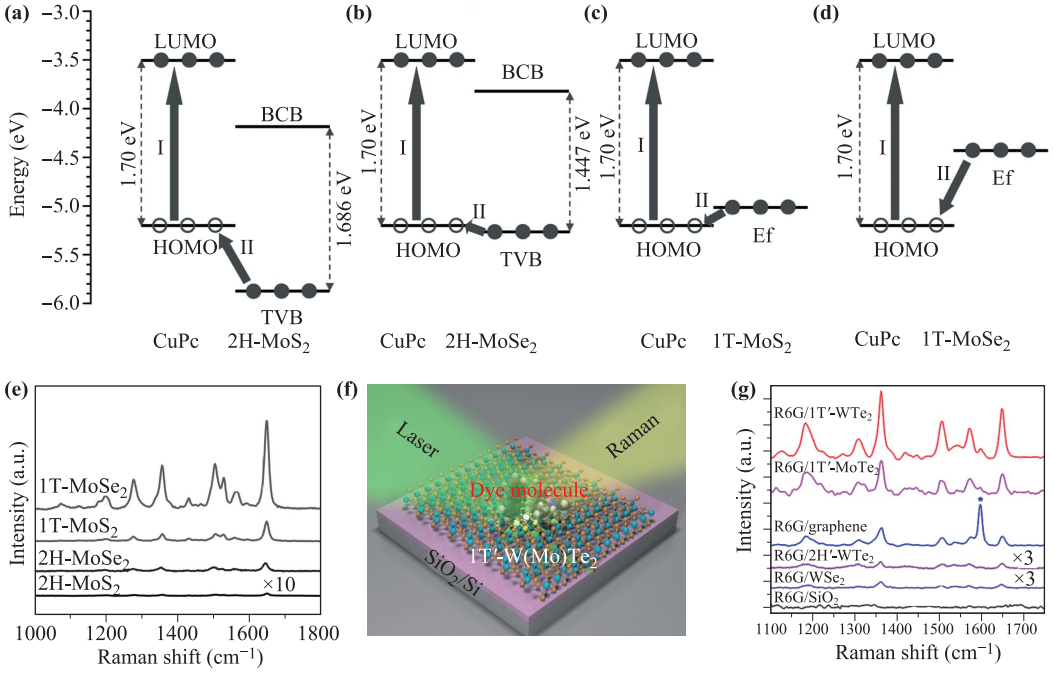

Fig. 6 Ultrasensitive SERS substrates are obtained by using phase engineering on MoX_2 (X=S, Se) and W(Mo)Te_2. **(a–d)** Schematic illustration of the energy band diagrams and CT process from 2H/1T-MoX_2 (X = S, Se) monolayer to CuPc. **(e)** SERS spectra of R6G adsorbed on 2H/1T-MoX_2 (X = S, Se) monolayer. **(f)** SERS effects on the 1T′-W(Mo)Te_2. **(g)** SERS spectra of R6G coated on 1T′-W(Mo)Te_2 and other substrates. Reproduced with permission from (a–e) Ref. [27], and (f and g) Ref. [25], Copyright © 2017 Wiley-VCH, Copyright © 2018 American Chemical Society.

as effective CT, therefore they may become promising candidates for high-performance SERS materials. Yin *et al.* reported the SERS properties of liquid exfoliation-obtained monolayer 2H-MoS_2, 2H-$MoSe_2$, 1T-MoS_2 and 1T-$MoSe_2$ [Figs. 6(a)–(e)] [27]. When the phase was transformed form 2H- to 1T-phase, the Raman enhancement of molecules adsorbed on MoX_2 (X=S, Se) monolayers can increase significantly. For semiconducting 2H-MoX_2, electrons can transfer from the VB of 2H-MoX_2 to HOMO level of CuPc molecules with enough extra energy. Compared with 2H-MoX_2, metallic 1T-MoX_2 possesses larger available DOS between the levels of HOMO and Fermi energy, which induces highly efficient CT from the Fermi energy level of 1T-MoX_2 to HOMO level of CuPc without requiring extra energy. Thus, larger enhancement in SERS was found in metallic 1T-MoX_2. Besides, Tao *et al.* confirmed that atomic layers of semimetallic 1T′-W(Mo)Te_2 can significantly enhance the signals of the R6G and achieve a remarkable LOD of 10^{-14} (10^{-13}) M [Figs. 6 (f, g)] [25]. For 1T′-W(Mo)Te_2, the EM contribution is excluded since the LSPR of W(Mo)Te_2 is located in the mid-infrared region. The strong interaction between the analyte and 1T′-W(Mo)Te_2 as well as abundant DOS near the Fermi level of 1T′-W(Mo)Te_2 lead to the prominent SERS effect by promoting the CT resonance in the analyte-W(Mo)Te_2 system. Other metallic/semimetallic TMDs SERS materials such as ReS_2 [28] and NbS_2 [26] have also been reported. In addition, Miao *et al.* demonstrated that the phase transition induced Raman enhancement on VO_2 nanosheets [153]. During the high temperature annealing process, monoclinic VO_2(B) could transform to another monoclinic VO_2(M) and to highly ordered tetragonal rutile VO_2(R). Among these phase structures, low crystal symmetry of VO_2(B) exhibits highest SERS activity and achieves a 10^{-7} M level detection limit for various dye molecules.

3.4 Heterojunction engineering

Heterojunction engineering has drawn intense research attention because it can provide multifunctional and enhanced properties that cannot be achieved by the individual material [154–157]. Recently, researchers introduce heterojunction engineering into the plasmon-free SERS fields, providing a brand-new way to obtain ultrasensitive plasmon-free SERS substrates [61, 67, 68, 158]. For example, our group designed a $W_{18}O_{49}$/monolayer MoS_2 (W/M) vertical heterojunction as an ultrasensitive SERS substrate [Figs. 7(a)–(c)] [67]. The substrate was successfully fabricated by coating a $W_{18}O_{49}$ thin layer on chemical vapor deposition (CVD)-grown monolayer MoS_2 via magnetron sputtering then annealing under hydrogen atmosphere. It was confirmed that the coupling of these two materials could lead to dramatic enhancement

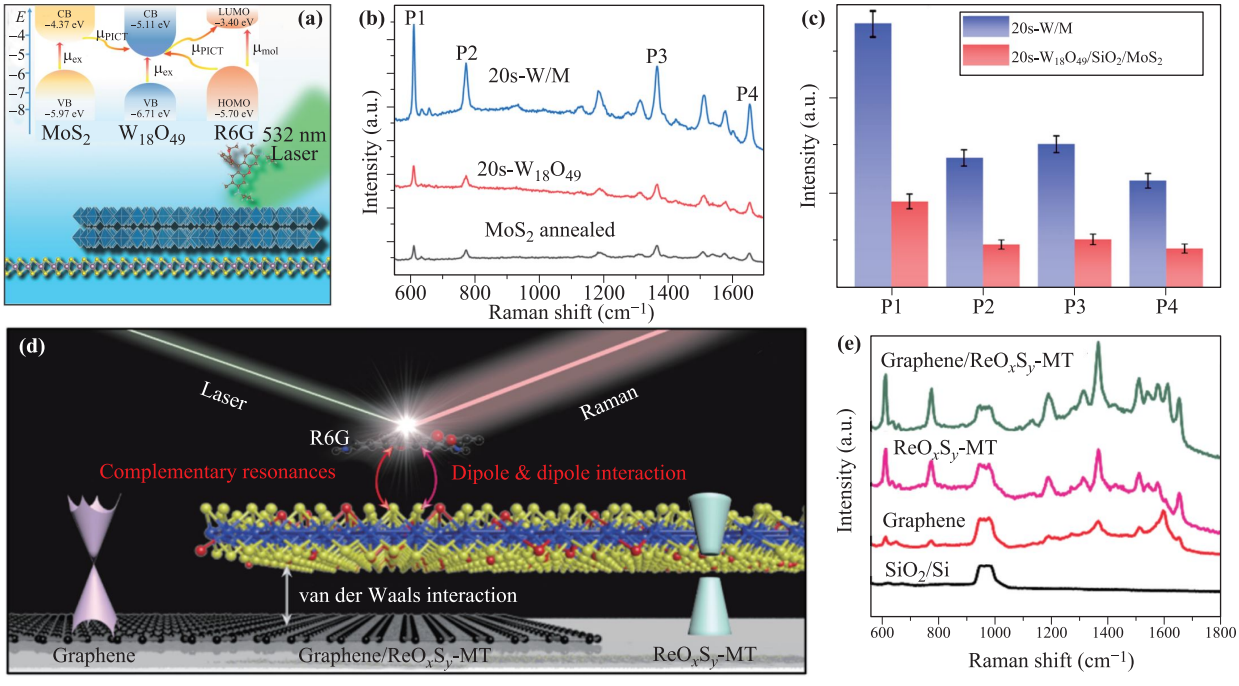

Fig. 7 Ultrasensitive SERS substrates are obtained by using heterojunction engineering on W/M and graphene/ReO_xS_y. **(a)** Schematic energy level diagrams and CT in the R6G-W/M ternary system. **(b)** SERS spectra of R6G adsorbed on the annealed monolayer MoS_2, $W_{18}O_{49}$, and W/M substrates. **(c)** SERS spectral comparison chart of R6G adsorbed on the W/M and $W_{18}O_{49}/SiO_2/MoS_2$ substrates. **(d)** Illustration of measured Raman enhancement of R6G on graphene/ReO_xS_y films. **(e)** SERS spectra of R6G adsorbed on graphene, ReO_xS_y, and graphene/ReO_xS_y substrates. Reproduced with permission from (a–c) Ref. [67] and (d, e) Ref. [61], Copyright © 2019–2020 American Chemical Society.

of PICT processes. The LOD for R6G molecule on W/M substrate is as low as 1 $\times 10^{-9}$ M with the maximum EF up to 3.45 $\times 10^{7}$. The EM enhancement is not considered because the LSPR of $W_{18}O_{49}$ is located at the mid-infrared region. According to the Raman spectra, there is considerable Raman enhancement under the wavelengths of 532 nm, while no detectable Raman signals exist at 633 and 785 nm excitation, indicating that Raman enhancement on the W/M substrate is a selective process by the CT mechanism. On the one hand, the internal properties of the W/M substrate promote efficient separation of electron–hole pairs and charge transformations, which could significantly improve the electron density on the surface of the substrate in contact with the adsorbed molecules. On the other hand, there are more possible exciton resonance transitions in the heterojunction structure. These synergistic effects could dramatically enhance the CT processes, which could outstandingly increase the SERS sensing capacity of W/M vertical heterojunction substrates. The black TiO_2 nanoparticle with crystal-amorphous core-shell heterojunction has been reported as a SERS substrate by Lin *et al.* [159]. Benefitting from the synergistic effects of the novel crystal-amorphous core-shell structure, this substrate shows a LOD of 10^{-6} M and a high EF value of 4.3 $\times 10^{5}$. High-efficiency exciton transitions in the crystal core can generate plentiful excitons, which can provide sufficient charge source. Subsequently, the heterojunction structure enables the efficient exciton separation at the interface of crystal-amorphous, which can effectively facilitate the CT from crystal core to amorphous shell and result in exciton enrichment at the amorphous shell. Besides, it was further confirmed that the amorphous shell structure possesses lower Fermi level position, narrower band gap, and higher DOS than crystal core. These features can offer effective routes of CT as well as strong vibronic coupling in TiO_2-analyte system, which are prominent in subsequent SERS enhancement. Similarly, other heterojunction structures, such as MoS_2/ZnO [160], graphene/ReO_xS_y [Figs. 7(d) and (e)] [61], graphene/WSe_2 [68], and InAs/GaAs [161] are also investigated. These multitudinous heterojunction substrates provide excellent platforms for ultrasensitive SERS sensing. Table 2 shows the summary of the reported plasmon-free SERS substrates obtained by heterojunction engineering in recent years.

3.5 Facet engineering

As an effective strategy for tuning the properties of nanomaterials, facet engineering has been applied in catalysis, gas sensors, and energy storage [179–181]. Nanomaterials with the selective exposure of facets exhibit distinctive surface electronic structures and surface electron transport properties due to the diverse atomic coordination and

Table 2 The summary of the reported plasmon-free SERS substrates obtained by heterojunction engineering in recent years.

Substrate	Probe	LOD (M)	EF	Ref.
2D $W_{18}O_{49}/MoS_2$	R6G	1 $\times 10^{-9}$	3.45 $\times 10^{7}$	[67]
TiO_2 core-shell nanoparticle	R6G	10^{-6}	4.3 $\times 10^{5}$	[159]
2D graphene/ReO_xS_y	R6G	1 $\times 10^{-14}$	N/A	[61]
2D graphene/WSe_2	CuPc	N/A	78.2	[68]
2D TMD/$SnSe_2$	TMD	N/A	10	[162]
1T/2H-MoS_2 nanosheet	R6G	5 $\times 10^{-8}$	N/A	[163]
1T/2H-WS_2 nanosheet	R6G	5 $\times 10^{-8}$	N/A	[163]
InAs/GaAs QDs	Pyridne	N/A	~10^{3}	[161]
Ag_2S/graphene oxide (GO) nanoparticle/sheet	Ag_2S/GO	N/A	N/A	[164]
ZnS/GO nanoparticle/sheet	4-Mpy	1 $\times 10^{-5}$	N/A	[165]
SiO_2/TiO_2 core-shell	Glutathione	$< 1 \times 10^{-3}$	N/A	[166]
GO/TiO_2 inverse opal	MB	6 $\times 10^{-7}$	5 $\times 10^{4}$	[167]
GO/TiO_2 nanocomposite	CuPc	N/A	48.2	[168]
GO/ZnO nanocomposite	R6G	1 $\times 10^{-10}$	7 $\times 10^{4}$	[169]
TiO_2-carbonaceous nanotube	MB	N/A	3 $\times 10^{3}$	[170]
Reduced graphene oxide (rGO)-TiO_2 nanoparticle/sheet	4-MBA	1 $\times 10^{-7}$	5.5 $\times 10^{6}$	[171]
rGO-TiO_2-Fe_3O_4 nanoparticle/sheet	4-MBA	1 $\times 10^{-10}$	2.7 $\times 10^{7}$	[172]
Fe_3O_4@GO@TiO_2 nanoparticle	CuPc	N/A	8.08 $\times 10^{6}$	[173]
ZnO/ZnS/MoS_2 nanoparticle	R6G	1 $\times 10^{-9}$	1.4 $\times 10^{8}$	[174]
MoS_2/ZnO nanoflower/particle	MB	1 $\times 10^{-12}$	1.13 $\times 10^{6}$	[175]
MoS_2/ZnO microflower/particle	Bisphenol A	1 $\times 10^{-9}$	5.8 $\times 10^{5}$	[176]
Graphene/MoS_2 nanoflower/sheet	Rhodamine B	5 $\times 10^{-11}$	2.96 $\times 10^{7}$	[177]
$CsPbBr_3$@ZIF-8 composite	4-Mpy	N/A	1.17 $\times 10^{5}$	[178]

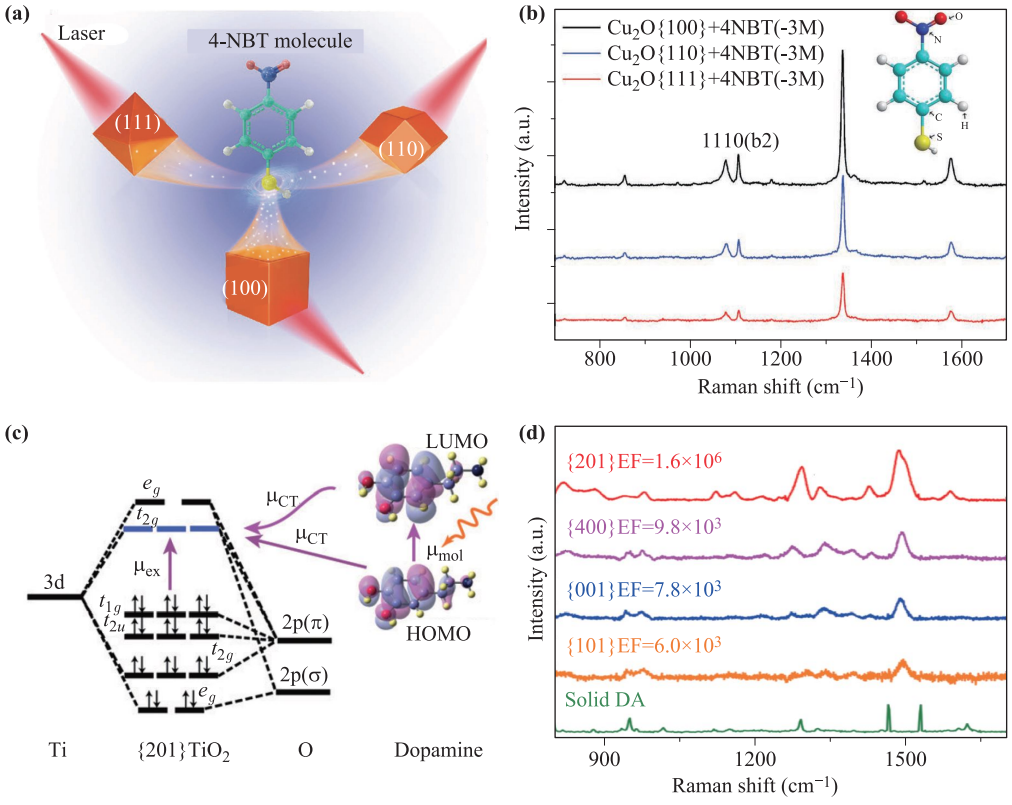

Fig. 8 Ultrasensitive SERS substrates are obtained by using facet engineering on Cu_2O and TiO_2. **(a)** Schematic illustration of CT process in the SERS effect of the three Cu_2O polyhedra. **(b)** SERS spectra of 4-nitrobenzenethiol obtained on three Cu_2O polyhedra. **(c)** Molecular-orbital diagram for {201} TiO_2 and DA molecule. **(d)** SERS spectra of DA on different TiO_2 and solid DA. Reproduced with permission from (a and b) Ref. [69], and (c and d) Ref. [70], Copyright © 2018 Wiley-VCH, Copyright © 2019 The Royal Society of Chemistry.

configurations. Recently, facet engineering has been used for improving the SERS behavior of plasmon-free materials [69, 70]. For example, compared with much less affinity for the {101} TiO_2, Urdaneta *et al.* reported a selective adsorption of dopamine (DA) on the {001} and {100} terminations, which was consistent with the CT associated to the SERS effect [182]. Guo *et al.* synthesized three different facets of Cu_2O microcrystals: {100}-cubic Cu_2O, {110}-octahedral Cu_2O, and {111}-dodecahedral Cu_2O [Figs. 8(a) and (b)] [69]. Among these Cu_2O microcrystals, {100} Cu_2O exhibited the strongest Raman signals. In {100} Cu_2O, Kelvin probe force microscopy (KPFM) technology and first-principle DFT calculation evidenced the highest interfacial CT based on the facet-dependent work function. More efficient CT process in {100} Cu_2O was obtained as its lowest electronic work function, resulting in the largest magnification of Raman scattering cross section. It is also worth mentioning that Yu *et al.* obtained a high EF of 1.6×10^6 from DA molecules adsorbed on a symmetric prickly {201} TiO_2, which is three orders of magnitude higher than that on asymmetric {001}, {101}, and {100} TiO_2 [Fig. 8(c) and (d)] [70]. Through combining XANES analysis, they demonstrated that the high density of unoccupied t_{2g} orbitals in {201} TiO_2 played a crucial role in efficient CT process, which made the CT of {201} TiO_2 1.3–1.8 times higher than others. In addition, electronic DOS calculations also demonstrated that the urchin-like spheres of {201} TiO_2 could generate a strong electromagnetic field enhancement, which further contributes to the Raman enhancement in DA-{201} TiO_2 system. Zhang *et al.* also reported that the SERS activity of TiO_2 could be improved by optimizing the exposed ratio between the {001} and {101} facets [183]. They found that the SERS performance was correlated with the enhanced mobility of photo-induced electrons on exposed {001} facets, which was promoted by the surface electric field pointing from exposed {101} facets to the junction edge, and then to {001} facets because of the heterogeneous facets potentials. So far, facet-dependent SERS materials almost are confined to metal oxides, it is possible to improve the SERS activity of non-metal-oxide materials by using facet engineering.

3.6 Molecular engineering

Π-conjugated organic small molecules that consist of π-conjugated moieties and functional groups have been widely used in optoelectronic devices as their structural

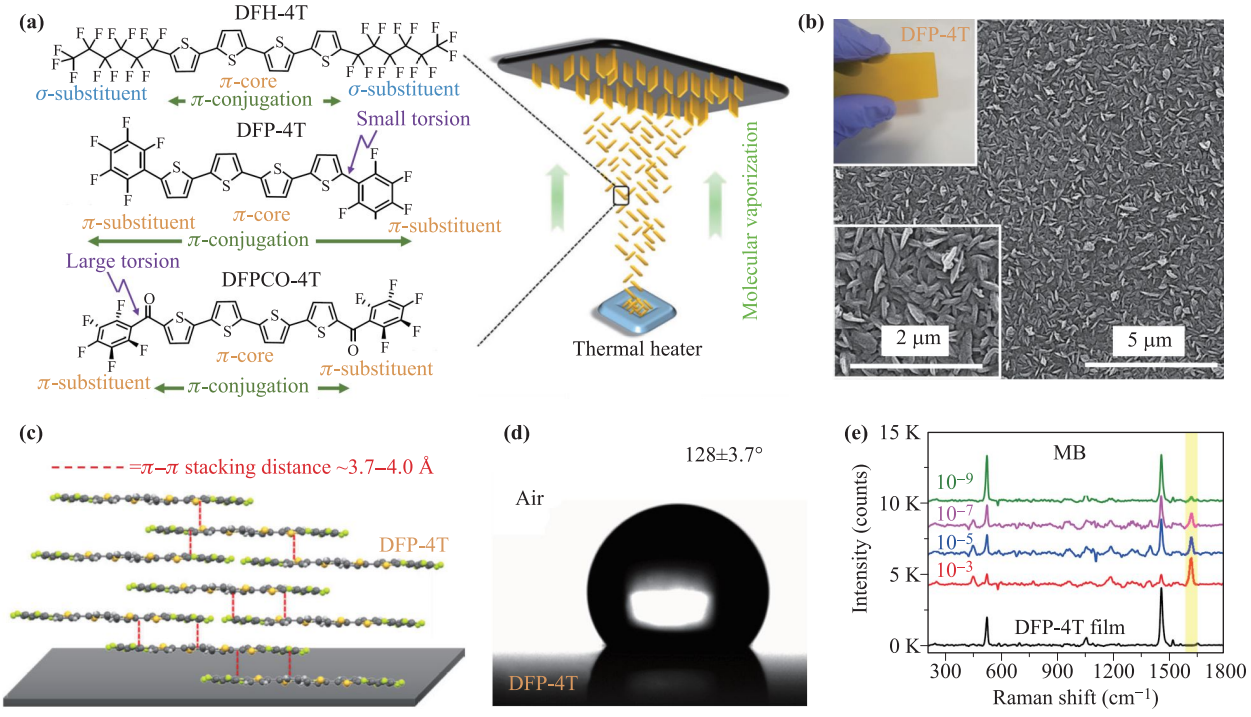

Fig. 9 **(a)** Chemical structures of the 4T-based semiconductors and schematic illustration of the preparation process for nanostructured films, **(b)** SEM images, **(c)** molecular packing diagram in the out of plane direction, **(d)** contact-angle of DFP-4T films, and **(e)** The SERS spectra of MB probe on DFP-4T films at different concentrations. Reproduced with permission from Ref. [47], Copyright © 2019 Springer Nature.

diversity, facile synthesis, and highly delocalized molecular orbitals [184]. Different from the molecules only with σ-electrons, the presence of delocalized π-electrons in π-conjugated organic semiconductors allows more exceptional charge transport or light manipulation properties. In 2017, Yilmaz *et al.* designed a novel SERS platform based on a,w-diperfluorohexylquaterthiophene (DFH-4T) thin film via an oblique-angle vapor deposition [46]. This superhydrophobic and ivy-like nanostructured organic film possesses a Raman EF of 3.4×10^3 for MB as the probe molecule. Theoretical calculation and contrast experiment indicate that the π-conjugated core fluorocarbon substitution and the unique DFH-4T film morphology facilitate intermolecular CT between the organic semiconductor and the probe molecule. This finding provides a new material for design plasmon-free SERS substrates, which is the first time for π-conjugated organic small molecule film enhancing Raman signals in the plasmon-free SERS filed. Subsequently, Demirel *et al.* reported a nanostructured film of the small molecule DFP-4T, consisting of a fully π-conjugated diperfluorophenyl-substituted quaterthiophene structure (Fig. 9). Compared with 5,5-di(per-fluorophenylcarbonyl)-2,2′:5′,2:5,2-quaterthiophene (DFPCO-4T) and DFH-4T film, the DFP-4T film exhibited a remarkable SERS sensitivity with a high EF exceeding 10^5 and a low LOD of 10^{-9} M for MB molecule [47]. According to the experimental and theoretical results, two conditions are required to satisfy for achieving high-performance SERS activity in organic semiconductors. One is that there exists small but nonzero oscillator strength in the CT state between the organic semiconductors and probe molecules, and the other is CT energy should be close to incident light to realize the resonance enhancement. It is expected to further improve the SERS activity of organic semiconductors by using chemical doping or electrical charge-injection which could tailor band edges and introduce free carrier into semiconductor structures. Simultaneously, as their structural flexibility and high tunability, organic semiconductors may achieve selective SERS detection toward specific analytes by adjusting their functional group and π-backbone length.

3.7 Other strategies

Additionally, other strategies that benefit to the performance of plasmon-free SERS substrates were proposed. As an example, Miao *et al.* reported the layer-number-dependent Raman enhancement effect on 1T′ phase ReS_2 [28]. It is found that the layer numbers from few-layer to monolayer can significantly strengthen the Raman enhancement effect on ReS_2 because the ReS_2 undergoes an indirect to direct band gap transition. As a result, monolayer ReS_2 exhibits ultrasensitive SERS activity and the LOD of R6G as low as 10^{-9} M. For monolayer ReS_2, the direct band gap allows excited electrons in CB to be immediately recombined with trapped hole carries, which is conducive to fluorescence quenching of dye molecules and CT process in molecule-ReS_2 system. How-

ever, in the terms of few-layer ReS_2, although the band gap shrinks slightly, the transition from the direct band gap to the indirect band gap may prolong the lifetime of excited electrons in the CB, resulting in a smaller difference in the chemical potential between probe molecules and ReS_2, which suppresses the CT process from the LUMO of molecules to the CB of ReS_2. Hu *et al.* demonstrated that electric field control of the SERS effect by adjusting the hole concentration of Sb:Na [139]. In the experiment, they dripped dye molecules onto the fabricated Sb:Na QDs-based field effect transistor (FET) device and observed the SERS effect *in situ*. More holes are injected into the FET device by applying different gate voltages, which enhances the SERS effect by boosting the CT between the molecules and Sb:Na QDs, bringing the LOD to the sub-femtomolar level. Similarly, Zhou *et al.* reported an electrically tunable SERS substrate based on WO_{3-x} films [185]. The EF of which can increase from 3.01 $\times 10^5$ to 1.14 $\times 10^6$ by electrical programming of the defect density through the oxide leakage current control. Besides, highly tailorable MOFs have been used as SERS substrates with a low LOD of 10^{-8} M and a high EF of ~10^5, reported by Zhao *et al.* [42]. By adjusting the metal centers and organic ligands, the electronic band structures of the MOF-based SERS substrates could be purposively manipulated to match that of the target analyte, thus resulting in the combination of several resonances and subsequent prominent SERS enhancement. Further, by adjusting the LUMO and HOMO levels of ZIF-67 through a doping process with different metal ions, Xu *et al.* fabricated a flexible and reusable SERS substrate with a high EF (6.07 $\times 10^6$) [45]. Li *et al.* reported that surface-modified 2D Ti_3C_2 sheets, as SERS substrates, possess highly sensitive but nonselective enhancement with the detection limit down to the pM level [53]. The Raman signals of MB molecule adsorbed on Ti_3C_2-$Al(OH)_4$ sheets is four orders of magnitude higher than that of Ti_3C_2-OH/F sheets. The enhanced SERS activity could be attributed to the strong but nonselective interactions between substrate and analyte, which is induced by the surface aluminum oxyanion groups. With the aluminum oxyanion groups closely and evenly pack on the sheet surface, the analytes could adopt a configuration similar to that on a blank substrate, lying flat with C-N slightly distorted toward the substrate, which allows the unusual combination of ultrasensitive enhancement of signals and no obvious preference among different vibrational modes. Lin *et al.* proposed a low temperature-based strategy to facilitate the PICT processes and improve semiconductor SERS activity [130]. They found that the Raman intensity of 4-Mpy molecule adsorbed on porous ZnO nanosheets with abundant surface defect states is enhanced about 4 times at a 77 K compared to that at room temperature. Low-temperature condition could provide an ideal environment to reduce phonon-assisted relaxation and weaken lattice thermal vibration, thereby reducing the non-radiative recombination of excitons and increasing the number of photo-induced electrons to participate in the PICT processes. Finally, a low LOD of 1×10^{-7} M and a high EF of 7.7 $\times 10^5$ for 4-Mpy molecules are obtained at a low temperature of 77 K. Zhao *et al.* reported that high pressure could promote the CT efficiency and change the intensity of Raman signal in the semiconductor-molecule system [186, 187]. In addition, Li *et al.* investigated the effect of MoS_2 interlayer distances on the SERS activity of MoS_2 [188]. They found that MoS_2 with smaller interlayer distances shows stronger SERS enhancement and an EF as high as 5.31 $\times 10^5$ could be achieved in MoS_2-0.62 (interlayer distance is 0.62 nm). In a word, these strategies not only provide a deep insight of the enhancement mechanisms for plasmon-free SERS materials, but also open up the way for preparation and application of plasmon-free SERS materials.

4 The applications of plasmon-free SERS

4.1 Biomedical diagnosis

Biomedical diagnosis with SERS is an effective diagnostic method because it is ultrasensitive, non-destructive, and capable of real-time molecular detection. Compared to noble metals, plasmon-free materials show superior biocompatibility and high stability [189, 190]. Furthermore, plasmon-free materials can form stable coordination bonds with the carboxyl and amine groups of biomolecules, maintaining their biological activity. Therefore, plasmon-free SERS is a promising method for biomedical diagnosis. Haldavnekar *et al.* obtained a ZnO-based semiconductor quantum SERS probe using femtosecond pulsed laser processing [129]. Owing to the surface oxygen vacancies and stacking faults, the probes could achieve the EF ~10^6 with LOD down to 10^{-9} M. The ratio of peak intensities of lipids and proteins were used to distinguish between cancer and non-cancer. In this way, the probes achieve label-free, in vitro SERS diagnosis of cancer with a single-cell-level detection (Fig. 10). Apart from that, the organic semiconductor SERS sensor has been served for the detection of deoxyribonucleic acid (DNA) methylation and gene expression [191]. The reported organic semiconductor SERS sensor shows ultrasensitive SERS detectivity, which could detect the genomic DNA even at femtomolar concentration. We know that the genomic DNA can provide the information about the structural, molecular, and gene expression changes of DNA. In this case, this SERS sensor can be used for diagnosing the cancer stem cells by analyzing the differences between the genomic DNA of cancerous and non-cancerous cells. Besides, Lin *et al.* fabricated black TiO_2 nanoparticle that could enhance Raman scattering with the EF 4.3 $\times 10^5$ [159]. On the one hand, the black TiO_2 nanoparticle could be applied to SERS mapping imaging technology, which has been employed to accurately diagnose the MCF-7 drug-

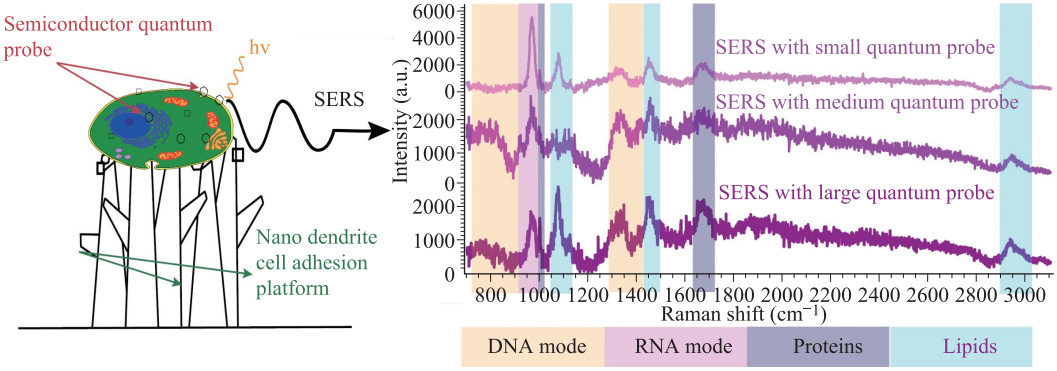

Fig. 10 Different sizes of plasmon-free semiconductor quantum SERS probes as the platforms for in vitro cell detection. Reproduced with permission from Ref. [129], Copyright © 2018 Springer Nature.

resistant breast cancer cells. On the other hand, with excellent photothermal conversion efficiency, the black TiO_2 nanoparticle could also act as a promising heat mediator for efficient photothermal ablation of the cancer cells. Capable of detecting different gaseous indicators of lung cancer with ppm detection limit, the MIL-100(Fe) SERS platform proposed by Fu *et al.* shows great potential for screening and clinical diagnosis of lung cancer in the early stage [44]. In addition, Tian *et al.* reported that functionalized hexagonal boron nitride nanosheets could be used as a SERS platform for real-time monitoring and imaging of microRNA [39]. All these works indicate that plasmon-free SERS substrates have a bright prospect in cell labeling and imaging, biological diagnosis, photothermal therapy and so on.

4.2 Metal ions and organic pollutants sensing

Metal ions and organic pollutants sensing have aroused wide concern for their strong environmental and biomedical impact [192]. Fortunately, the selectivity and reusability of plasmon-free SERS substrates provide excellent platforms for metal ions and organic pollutants sensing. One case is the "turn-off" SERS strategy for metal ion detection proposed by Ji *et al.* [193]. Wherein the stable and highly reproducible SERS intensity of alizarin red S (ARS)-TiO_2 complexes was borrowed from the efficient CT process that results from the vibronic coupling between the excited molecular level and the CB of TiO_2. They found that the SERS intensities of the complexes are sensitive to the Cr(VI) concentration due to co-catalysis, and the LOD of 0.5 μM Cr(VI) cations has been achieved. Furthermore, the complexes exhibit a remarkably high selectivity toward Cr(VI) cations, which originates from the energy level matching between the redox potential of Cr(VI)/Cr(V) and the energy level of the TiO_2. Our group also prepared a series of transition metal oxide chips by a general strategy based on magnetron sputtering with H_2 annealing treatment. Successfully, these chips could selectively improve the signals of specific organic pollutant in the detected mixture solutions [105]. In the terms of practical application, plasmon-free materials could be used as recyclable SERS substrates owing to their self-cleaning ability by photo-degrading the organic pollutants. Majee *et al.* applied few-layer MoS_2 as a SERS substrate for the ultrasensitive detection of organic compounds at nanomolar level [194]. And, the treatment of adsorbed organic compounds over few-layer MoS_2 under visible light illumination has also been demonstrated to verify the reusability of the SERS substrate with repeated detectability.

4.3 Chemical and biochemical reactions monitoring

Typically, as a powerful approach for monitoring chemical and biochemical reactions, plasmon-free SERS has been used for studying surface/interface redox reactions, molecular adsorption, electrochemical reactions kinetics, and so on [195]. For example, with the help of electrochemical anodization of titanium, Han *et al.* prepared nanostructured TiO_2 electrodes and altered the Raman EF of cyt b_5 adsorbed on TiO_2 electrodes by adjusting the surface roughness with different anode voltages [196]. According to the SERS spectra measured at different electrode potentials, the protein oxidation marker band $\nu 4$ located in 1374 cm^{-1} (oxidized state) shifted to 1360 cm^{-1} (reduced state), indicating a redox protein process has happened. Alessandri *et al.* demonstrated that SiO_2–TiO_2 core-shell colloidal crystals can be used as a SERS probe to monitor the glutathione (L-γ-glutamyl-cysteinyl-glicine, GSH) redox cycle at physiological concentration in aqueous environment [197]. When GSH is oxidized to its disulphide derivative, the signal of –SH stretching would disappear in SERS spectrum. Thus, GSH oxidation process can be monitored by observing the –SH stretching Raman signal. Glass *et al.* reported that semiconductor-based SERS enhancements could be used as a direct method of surface oxygen vacancies concentration quantification [198]. Besides, our group reported that the oxidation process of ultraviolet-ozone-treated MoS_2 could be successfully mon-

itored by using plasmon-free SERS technology [134]. During the oxidation process, the changes in energy bands caused by defects in MoS_2 would remarkably affect SERS. Thus, we could quantify the degree of oxidation at different treatment time according to the exponential relationship between the percent of oxidation and treatment time obtained by SERS. Experimental and theoretical results indicate that MoS_2 is first doped with O_{ads}, then doped with O_s, and finally there forms a completely oxidized layer (MoO_3). Our study may provide a general strategy for tracking the oxidation and degradation process of other 2D materials.

4.4 Photoelectric characterization

Since that the intrinsic properties of plasmon-free SERS materials, such as the band structure and carrier concentration, affect the SERS property and other photoelectric characteristics of the materials, SERS measurement could be served as a tool to indirectly explore the photoelectric performance. Based on this point, Chen *et al.* monitored the carrier dynamics of π-conjugated polymer using SERS technology [199]. With poly(3,4-ethylenedioxythiophene):poly(styrenesulfonate) (PEDOT:PSS) as the plasmon-free SERS substrate, they discussed the Raman characterizations during the carrier dynamics process under different voltages and conductive situations. Due to abundant delocalized π electrons in PEDOT:PSS, the induced chemical enhancement causes high EF of the material. Furthermore, different bias voltages increased or reduced the carrier density of the PEDOT:PSS substrate, leading to the blue shift or red shift in Raman peaks respectively. This discovery provides an important theoretical fundament for the chemical enhancement model in SERS and offers a new idea for the researches on photoelectric devices. Similarly, Yu *et al.* constructed a photodetector device based on 4-Mpy-modified perovskite. The results demonstrated that a correlation between the CT resonance-enhanced Raman and the photoelectronic responses of perovskite materials [31]. By exploring the CT pathways of hybrid dye/molecule-metal oxide complexes via SERS, Tarakeshwar *et al.* discovered the close correlation between the Raman enhancement and the electron transfer rate on the molecule-TiO_2 interface, providing a significant guidance for the nature of CT paths [200]. Besides, Yang *et al.* contrasted the photoluminescence and SERS spectra of the molecules absorbed on ZnO with that on Nd-doped ZnO, proving that unique property of Nd^{3+} ions not only can improve the SERS signals but also can eliminate the SERS fluorescence background [124]. They put forward a new path for studying CT and explaining the fluorescence quenching. Coincidentally, Tao and his colleagues studied the fluorescence quenching of plasmon-free SERS materials and drew a conclusion that it is helpful for the Raman enhancement [25].

5 Summary and outlook

Plasmon-free substrates represent new frontier for SERS. There has been surprising and accelerated development of plasmon-free SERS over the past decade. In this review, we introduce the background, enhancement mechanisms, enhancement strategies, and applications of ultrasensitive SERS sensing beyond plasmonics. The background of SERS and the advantages of plasmon-free SERS are firstly stated, followed by the enhancement mechanisms of plasmon-free SERS. Then, we summarize numerous enhancement strategies for constructing ultrasensitive plasmon-free SERS substrates. After that, the promising application of plasmon-free SERS in various areas such as biomedical diagnosis, metal ions and organic pollutants sensing, chemical and biochemical reactions monitoring, and photoelectric characterization are summarized. Considering recent development on plasmon-free SERS, we propose some potential significant topics in the field: (i) developing new technologies to prepare the plasmon-free SERS substrates. Some technologies like solvothermal method [16], CVD [25], magnetron sputtering [64], electrochemical method [196] have been developed to obtain plasmon-free SERS substrates. However, these preparation processes are generally complicated, low-yield and expensive. It is necessary to fabricate ultrasensitive plasmon-free SERS substrates through a simple, convenient and large-scale approach, which is the basis of their wide applications. (ii) Exploring new strategies to improve the SERS activity of plasmon-free substrates. At present, plasmon-free SERS materials have shown high sensitivity by using different enhancement strategies, but there is still a big gap with noble metal materials whose EFs are even higher than ~10^{14} for single-molecule detection [201]. High-performance SERS substrates are still the key factor limiting the practical application of plasmon-free SERS. In addition, researchers recently reported that some noble metal-free materials such as metal oxides [202–209], metal carbides [9, 210] and metal nitrides [211–213] possess high charge carrier concentration, which could induce LSPR effect in the visible region [214]. Plasmon resonance together with CT resonance, exciton resonance, molecular resonance, and Mie resonance may further improve the SERS activity of noble metal-free materials under some specific conditions. (iii) Discovering novel plasmon-free SERS materials. In recent years, a series of novel plasmon-free SERS materials have been explored (TMDs, MOFs, MXenes, perovskites, organic semiconductors and so on) [25, 26, 29, 31, 32, 42, 43, 46, 47]. New materials not only can expand people's cognition of plasmon-free SERS materials, but also benefit further understanding of the enhancement mechanism. (iv) Expanding the application of plasmon-free SERS substrates. Plasmon-free SERS substrates with ultrahigh sensitivity have been reported in recent, showing the great potential

for replacing plasmonic noble metal substrates. It is worth noting that the high biocompatibility and low biological damage of plasmon-free SERS substrates have given them an inherent advantage in biochemical and biomedical sensing. Plasmon-free SERS can also be integrated into other techniques (IR spectroscopy, fluorescence spectroscopy, atomic force microscope, and so on) [215–217], which can achieve multiplexed analysis. Moreover, it may be a promising application direction of the plasmon-free SERS materials to combine novel plasmon-free materials with conventional noble metals [218–223]. This integration not only could enable a synergistic modulation of both the chemical and electromagnetic properties of the hybrid SERS platforms and obtain an ultrasensitive SERS activity, but also could take the advantages of both materials to achieve multifunctional applications.

Acknowledgements This work was supported by the National Natural Science Foundation of China (Grant No. 11874108) and the National Key R&D Program of China (Grant No. 2017YFA0403600).

References

1. M. Fleischmann, P. J. Hendra, and A. J. Mcquillan, Raman spectra of pyridine adsorbed at silver electrode, *Chem. Phys. Lett.* 26(2), 163 (1974)
2. D. L. Jeanmaire and R. P. Van Duyne, Surface Raman spectroelectrochemistry (Part I): Heterocyclic, aromatic, and aliphatic amines adsorbed on the anodized silver electrode, *J. Electroanal. Chem.* 84(1), 1 (1977)
3. M. G. Albrecht, and J. A. Creighton, Anomalously intense Raman spectra of phridine at a silver electrode, *J. Am. Chem. Soc.* 99(15), 5215 (1977)
4. C. Zong, M. X. Xu, L. J. Xu, T. Wei, X. Ma, X. S. Zheng, R. Hu, and B. Ren, Surface-enhanced Raman spectroscopy for bioanalysis: Reliability and challenges, *Chem. Rev.* 118(10), 4946 (2018)
5. X. Wang, S. C. Huang, S. Hu, S. Yan, and B. Ren, Fundamental understanding and applications of plasmon-enhanced Raman spectroscopy, *Nat. Rev. Phys.* 2(5), 253 (2020)
6. J. Langer, D. Jimenez De Aberasturi, J. Aizpurua, R. A. Alvarez-Puebla, B. Auguié, et al., Present and future of surface-enhanced Raman scattering, *ACS Nano* 14(1), 28 (2020)
7. Y. S. Yamamoto, M. Ishikawa, Y. Ozaki, and T. Itoh, Fundamental studies on enhancement and blinking mechanism of surface-enhanced Raman scattering (SERS) and basic applications of SERS biological sensing, *Front. Phys.* 9(1), 31 (2014)
8. X. C. Fan, Q. Hao, M. Z. Li, X. Y. Zhang, X. Z. Yang, Y. F. Mei, and T. Qiu, Hotspots on the move: Active molecular enrichment by hierarchically structured micromotors for ultrasensitive SERS sensing, *ACS Appl. Mater. Interfaces* 12(25), 28783 (2020)
9. L. L. Lan, X. C. Fan, Y. M. Gao, G. Q. Li, Q. Hao, and T. Qiu, Plasmonic metal carbide SERS chips, *J. Mater. Chem. C* 8(41), 14523 (2020)
10. Q. Hao, M. Z. Li, J. W. Wang, X. C. Fan, J. Jiang, X. X. Wang, M. S. Zhu, T. Qiu, L. B. Ma, P. K. Chu, and O. G. Schmidt, Flexible surface-enhanced Raman scattering chip: A universal platform for real-time interfacial molecular analysis with femtomolar sensitivity, *ACS Appl. Mater. Interfaces* 12(48), 54174 (2020)
11. X. Wang, S. C. Huang, T. X. Huang, H. S. Su, J. H. Zhong, Z. C. Zeng, M. H. Li, and B. Ren, Tip-enhanced Raman spectroscopy for surfaces and interfaces, *Chem. Soc. Rev.* 46(13), 4020 (2017)
12. Z. L. Zhang, L. Chen, S. X. Sheng, M. T. Sun, H. R. Zheng, K. Q. Chen, and H. X. Xu, High-vacuum tip enhanced Raman spectroscopy, *Front. Phys.* 9(1), 17 (2014)
13. J. F. Li, Y. F. Huang, Y. Ding, Z. L. Yang, S. B. Li, X. S. Zhou, F. R. Fan, W. Zhang, Z. Y. Zhou, D. Y. Wu, B. Ren, Z. L. Wang, and Z. Q. Tian, Shell-isolated nanoparticle-enhanced Raman spectroscopy, *Nature* 464(7287), 392 (2010)
14. Y. Q. Gu, C. He, Y. Q. Zhang, L. Lin, B. D. Thackray, and J. Ye, Gap-enhanced Raman tags for physically unclonable anticounterfeiting labels, *Nat. Commun.* 11(1), 516 (2020)
15. F. Z. Cong, H. Wei, X. R. Tian, and H. X. Xu, A facile synthesis of branched silver nanowire structures and its applications in surface-enhanced Raman scattering, *Front. Phys.* 7(5), 521 (2012)
16. L. L. Lan, X. Y. Hou, Y. M. Gao, X. C. Fan, and T. Qiu, Inkjet-printed paper-based semiconducting substrates for surface-enhanced Raman spectroscopy, *Nanotechnology* 31(5), 055502 (2020)
17. S. Cong, Y. Y. Yuan, Z. G. Chen, J. Y. Hou, M. Yang, Y. L. Su, Y. Y. Zhang, L. Li, Q. W. Li, F. X. Geng, and Z. G. Zhao, Noble metal-comparable SERS enhancement from semiconducting metal oxides by making oxygen vacancies, *Nat. Commun.* 6(1), 7800 (2015)
18. J. Lin, Y. Shang, X. X. Li, J. Yu, X. T. Wang, and L. Guo, Ultrasensitive SERS detection by defect engineering on single Cu_2O superstructure particle, *Adv. Mater.* 29(5), 1604797 (2017)
19. L. L. Yang, Y. S. Peng, Y. Yang, J. J. Liu, H. L. Huang, B. H. Yu, J. M. Zhao, Y. L. Lu, Z. R. Huang, Z. Y. Li, and J. R. Lombardi, A novel ultra-sensitive semiconductor SERS substrate boosted by the coupled resonance effect, *Adv. Sci.* 6(12), 1900310 (2019)
20. Y. F. Shan, Z. H. Zheng, J. J. Liu, Y. Yong, Z. Y. Li, Z. R. Huang, and D. L. Jiang, Niobium pentoxide: A promising surface-enhanced Raman scattering active semiconductor substrate, *npj Comput. Mater.* 3(1), 11 (2017)
21. D. Y. Qi, L. J. Lu, L. Z. Wang, and J. L. Zhang, Improved SERS sensitivity on plasmon-free TiO_2 photonic microarray by enhancing light-matter coupling, *J. Am. Chem. Soc.* 136(28), 9886 (2014)
22. J. T. Xu, X. T. Li, Y. X. Wang, R. H. Guo, S. M. Shang, and S. X. Jiang, Flexible and reusable cap-like thin Fe_2O_3 film for SERS applications, *Nano Res.* 12(2), 381 (2019)

23. C. Muehlethaler, C. R. Considine, V. Menon, W. C. Lin, Y. H. Lee, and J. R. Lombardi, Ultrahigh Raman enhancement on monolayer MoS_2, *ACS Photonics* 3(7), 1164 (2016)

24. Z. H. Zheng, S. Cong, W. B. Gong, J. N. Xuan, G. H. Li, W. B. Lu, F. X. Geng, and Z. G. Zhao, Semiconductor SERS enhancement enabled by oxygen incorporation, *Nat. Commun.* 8(1), 1993 (2017)

25. L. Tao, K. Chen, Z. F. Chen, C. X. Cong, C. Y. Qiu, J. J. Chen, X. M. Wang, H. Chen, T. Yu, W. G. Xie, S. Z. Deng, and J. B. Xu, 1T transition metal telluride atomic layers for plasmon-free SERS at femtomolar levels, *J. Am. Chem. Soc.* 140(28), 8696 (2018)

26. X. J. Song, Y. Wang, F. Zhao, Q. C. Li, H. Q. Ta, M. H. Rümmeli, C. G. Tully, Z. Z. Li, W. J. Yin, L. T. Yang, K. B. Lee, J. Yang, I. Bozkurt, S. W. Liu, W. J. Zhang, and M. Chhowalla, Plasmon-free surface-enhanced Raman spectroscopy using metallic 2D materials, *ACS Nano* 13(7), 8312 (2019)

27. Y. Yin, P. Miao, Y. M. Zhang, J. C. Han, X. H. Zhang, Y. Gong, L. Gu, C. Y. Xu, T. Yao, P. Xu, Y. Wang, B. Song, and S. Jin, Significantly increased Raman enhancement on MoX_2 (X = S, Se) monolayers upon phase transition, *Adv. Funct. Mater.* 27(16), 1606694 (2017)

28. P. Miao, J. K. Qin, Y. F. Shen, H. M. Su, J. F. Dai, B. Song, Y. C. Du, M. T. Sun, W. Zhang, H. L. Wang, C. Y. Xu, and P. Xu, Unraveling the Raman enhancement mechanism on 1T′-phase ReS_2 nanosheets, *Small* 14(14), 1704079 (2018)

29. C. C. Weng, Y. Y. Luo, B. F. Wang, J. P. Shi, L. Gao, Z. Y. Cao, and G. T. Duan, Layer-dependent SERS enhancement of TiS_2 prepared by simple electrochemical intercalation, *J. Mater. Chem. C* 8(40), 14138 (2020)

30. L. Quan, Y. Q. Song, Y. Lin, G. H. Zhang, Y. M. Dai, Y. K. Wu, K. Jin, H. Y. Ding, N. Pan, Y. Luo, and X. P. Wang, The Raman enhancement effect on a thin GaSe flake and its thickness dependence, *J. Mater. Chem. C* 3(42), 11129 (2015)

31. Z. Yu, W. L. Yu, J. Xing, R. A. Ganeev, W. Xin, J. L. Cheng, and C. L. Guo, Charge transfer effects on resonance-enhanced Raman scattering for molecules adsorbed on single-crystalline perovskite, *ACS Photonics* 5(4), 1619 (2018)

32. X. Y. Su, H. Ma, H. Wang, X. L. Li, X. X. Han, and B. Zhao, Surface-enhanced Raman scattering on organic-inorganic hybrid perovskites, *Chem. Commun.* 54(17), 2134 (2018)

33. X. Ling, L. M. Xie, Y. Fang, H. Xu, H. L. Zhang, J. Kong, M. S. Dresselhaus, J. Zhang, and Z. F. Liu, Can graphene be used as a substrate for Raman enhancement? *Nano Lett.* 10(2), 553 (2010)

34. S. M. Feng, M. C. dos Santos, B. R. Carvalho, R. T. Lv, Q. Li, K. Fujisawa, A. L. Elias, Y. Lei, N. Perea-Lopez, M. Endo, M. H. Pan, M. A. Pimenta, and M. Terrones, Ultrasensitive molecular sensor using N-doped graphene through enhanced Raman scattering, *Sci. Adv.* 2(7), e1600322 (2016)

35. H. Xu, L. M. Xie, H. L. Zhang, and J. Zhang, Effect of graphene Fermi level on the Raman scattering intensity of molecules on graphene, *ACS Nano* 5(7), 5338 (2011)

36. H. H. Tian, N. Zhang, J. Zhang, and L. M. Tong, Exploring quantification in a mixture using graphene-based surface-enhanced Raman spectroscopy, *Appl. Mater. Today* 15, 288 (2019)

37. R. Das, S. Parveen, A. Bora, and P. K. Giri, Origin of high photoluminescence yield and high SERS sensitivity of nitrogen-doped graphene quantum dots, *Carbon* 160, 273 (2020)

38. N. Zhang, L. M. Tong, and J. Zhang, Graphene-based enhanced Raman scattering toward analytical applications, *Chem. Mater.* 28(18), 6426 (2016)

39. J. Liu, T. T. Zhang, and Y. Tian, Functionalized h-BN nanosheets as a theranostic platform for SERS real-time monitoring of microRNA and photodynamic therapy, *Angew. Chem. Int. Ed.* 58(23), 7757 (2019)

40. X. Ling, W. J. Fang, Y. H. Lee, P. T. Araujo, X. Zhang, J. F. Rodriguez-Nieva, Y. X. Lin, J. Zhang, J. Kong, and M. S. Dresselhaus, Raman enhancement effect on two-dimensional layered materials: Graphene, h-BN and MoS_2, *Nano Lett.* 14(6), 3033 (2014)

41. Q. R. Cai, S. Mateti, W. R. Wang, R. Jones, K. Watanabe, T. Taniguchi, S. M. Huang, Y. Chen, and L. H. Li, Boron nitride nanosheets improve sensitivity and reusability of surface-enhanced Raman spectroscopy, *Angew. Chem. Int. Ed.* 55(29), 8405 (2016)

42. H. Z. Sun, S. Cong, Z. H. Zheng, Z. Wang, Z. G. Chen, and Z. G. Zhao, Metal-organic frameworks as surface enhanced Raman scattering substrates with high tailorability, *J. Am. Chem. Soc.* 141(2), 870 (2019)

43. T. H. Yu, C. H. Ho, C. Y. Wu, C. H. Chien, C. H. Lin, and S. Lee, Metal-organic frameworks: A novel SERS substrate, *J. Raman Spectrosc.* 44(11), 1506 (2013)

44. J. H. Fu, Z. Zhong, D. Xie, Y. J. Guo, D. X. Kong, Z. X. Zhao, Z. X. Zhao, and M. Li, SERS-active MIL-100(Fe) sensory array for ultrasensitive and multiplex detection of VOCs, *Angew. Chem. Int. Ed.* 59(46), 20489 (2020)

45. J. T. Xu, C. Cheng, S. M. Shang, W. Gao, P. Zeng, and S. X. Jiang, Flexible, reusable SERS substrate derived from ZIF-67 by adjusting LUMO and HOMO and its application in identification of bacteria, *ACS Appl. Mater. Interfaces* 12(44), 49452 (2020)

46. M. Yilmaz, E. Babur, M. Ozdemir, R. L. Gieseking, Y. Dede, U. Tamer, G. C. Schatz, A. Facchetti, H. Usta, and G. Demirel, Nanostructured organic semiconductor films for molecular detection with surface-enhanced Raman spectroscopy, *Nat. Mater.* 16(9), 918 (2017)

47. G. Demirel, R. L. M. Gieseking, R. Ozdemir, S. Kahmann, M. A. Loi, G. C. Schatz, A. Facchetti, and H. Usta, Molecular engineering of organic semiconductors enables noble metal-comparable SERS enhancement and sensitivity, *Nat. Commun.* 10(1), 5502 (2019)

48. J. J. Lin, L. B. Liang, X. Ling, S. Q. Zhang, N. N. Mao, N. Zhang, B. G. Sumpter, V. Meunier, L. M. Tong, and J. Zhang, Enhanced Raman scattering on in-plane anisotropic layered materials, *J. Am. Chem. Soc.* 137(49), 15511 (2015)

49. A. Kundu, R. Rani, and K. S. Hazra, Controlled nanofabrication of metal-free SERS substrate on few layered black phosphorus by low power focused laser irradiation, *Nanoscale* 11(35), 16245 (2019)
50. R. Wang, X. Y. Yan, B. C. Ge, J. X. Zhou, M. L. Wang, L. X. Zhang, and T. F. Jiao, Facile preparation of self-assembled black phosphorus-dye composite films for chemical gas sensors and surface-enhanced Raman scattering performances, *ACS Sustain. Chem. & Eng.* 8(11), 4521 (2020)
51. L. Hu, M. N. Amini, Y. Y. Wu, Z. Y. Jin, J. Yuan, R. B. Lin, J. H. Wu, Y. M. Dai, H. P. He, Y. F. Lu, J. G. Lu, Z. Z. Ye, S. T. Han, J. Ye, B. Partoens, Y. J. Zeng, and S. C. Ruan, Charge transfer doping modulated Raman scattering and enhanced stability of black phosphorus quantum dots on a ZnO nanorod, *Adv. Opt. Mater.* 6(15), 1800440 (2018)
52. T. B. Limbu, B. Chitara, J. D. Orlando, M. Y. G. Cervantes, S. Kumari, Q. Li, Y. A. Tang, and F. Yan, Green synthesis of reduced $Ti_3C_2T_x$ MXene nanosheets with enhanced conductivity, oxidation stability, and SERS activity, *J. Mater. Chem. C* 8(14), 4722 (2020)
53. G. H. Li, W. B. Gong, T. L. Qiu, S. Cong, Z. G. Zhao, R. Z. Ma, Y. Michiue, T. Sasaki, and F. X. Geng, Surface-modified two-dimensional titanium carbide sheets for intrinsic vibrational signal-retained surface-enhanced Raman scattering with ultrahigh uniformity, *ACS Appl. Mater. Interfaces* 12(20), 23523 (2020)
54. B. Soundiraraju and B. K. George, Two-dimensional titanium nitride (Ti_2N) MXene: Synthesis, characterization, and potential application as surface-enhanced Raman scattering substrate, *ACS Nano* 11(9), 8892 (2017)
55. A. Sarycheva, T. Makaryan, K. Maleski, E. Satheeshkumar, A. Melikyan, H. Minassian, M. Yoshimura, and Y. Gogotsi, Two-dimensional titanium carbide (MXene) as surface-enhanced Raman scattering substrate, *J. Phys. Chem. C* 121(36), 19983 (2017)
56. K. Y. Chen, X. Y. Yan, J. K. Li, T. F. Jiao, C. Cai, G. D. Zou, R. Wang, M. L. Wang, L. X. Zhang, and Q. M. Peng, Preparation of self-assembled composite films constructed by chemically-modified MXene and dyes with surface-enhanced Raman scattering characterization, *Nanomaterials (Basel)* 9(2), 284 (2019)
57. S. Elumalai, J. R. Lombardi, and M. Yoshimura, The surface-enhanced resonance Raman scattering of dye molecules adsorbed on two-dimensional titanium carbide $Ti_3C_2T_x$ (MXene) film, *Mater. Adv.* 1(2), 146 (2020)
58. Y. S. Peng, P. Cai, L. L. Yang, Y. Y. Liu, L. F. Zhu, Q. Q. Zhang, J. J. Liu, Z. R. Huang, and Y. Yang, Theoretical and experimental studies of Ti_3C_2 MXene for surface-enhanced Raman spectroscopy-based sensing, *ACS Omega* 5(41), 26486 (2020)
59. I. Alessandri and J. R. Lombardi, Enhanced Raman scattering with dielectrics, *Chem. Rev.* 116(24), 14921 (2016)
60. X. L. Wu, S. J. Xiong, Z. Liu, J. Chen, J. C. Shen, T. H. Li, P. H. Wu, and P. K. Chu, Green light stimulates terahertz emission from mesocrystal microspheres, *Nat. Nanotechnol.* 6(2), 103 (2011)
61. J. Seo, J. Lee, Y. Kim, D. Koo, G. Lee, and H. Park, Ultrasensitive plasmon-free surface-enhanced Raman spectroscopy with femtomolar detection limit from 2D van der Waals heterostructure, *Nano Lett.* 20(3), 1620 (2020)
62. X. X. Han, W. Ji, B. Zhao, and Y. Ozaki, Semiconductor-enhanced Raman scattering: Active nanomaterials and applications, *Nanoscale* 9(15), 4847 (2017)
63. N. Chen, T. H. Xiao, Z. Y. Luo, Y. Kitahama, K. Hiramatsu, N. Kishimoto, T. Itoh, Z. Z. Cheng, and K. Goda, Porous carbon nanowire array for surface-enhanced Raman spectroscopy, *Nat. Commun.* 11(1), 4772 (2020)
64. X. C. Fan, M. Z. Li, Q. Hao, M. S. Zhu, X. Y. Hou, H. Huang, L. B. Ma, O. G. Schmidt, and T. Qiu, High SERS sensitivity enabled by synergistically enhanced photoinduced charge transfer in amorphous non-stoichiometric semiconducting films, *Adv. Mater. Interfaces* 6(19), 1901133 (2019)
65. X. T. Wang, W. X. Shi, Z. Jin, W. F. Huang, J. Lin, G. S. Ma, S. Z. Li, and L. Guo, Remarkable SERS activity observed from amorphous ZnO nanocages, *Angew. Chem. Int. Ed.* 56(33), 9851 (2017)
66. X. T. Wang, W. X. Shi, S. X. Wang, H. W. Zhao, J. Lin, Z. Yang, M. Chen, and L. Guo, Two-dimensional amorphous TiO_2 nanosheets enabling high-efficiency photoinduced charge transfer for excellent SERS activity, *J. Am. Chem. Soc.* 141(14), 5856 (2019)
67. M. Z. Li, X. C. Fan, Y. M. Gao, and T. Qiu, $W_{18}O_{49}$/Monolayer MoS_2 heterojunction-enhanced Raman scattering, *J. Phys. Chem. Lett.* 10(14), 4038 (2019)
68. Y. Tan, L. N. Ma, Z. B. Gao, M. Chen, and F. Chen, Two-dimensional heterostructure as a platform for surface-enhanced Raman scattering, *Nano Lett.* 17(4), 2621 (2017)
69. J. Lin, W. Hao, Y. Shang, X. T. Wang, D. L. Qiu, G. S. Ma, C. Chen, S. Z. Li, and L. Guo, Direct experimental observation of facet-dependent SERS of Cu_2O polyhedra, *Small* 14(8), 1703274 (2018)
70. Y. Q. Yu, J. J. Du, and C. Y. Jing, Remarkable surface-enhanced Raman scattering on self-assembled [201] anatase, *J. Mater. Chem. C* 7(45), 14239 (2019)
71. X. X. Li, Y. Shang, J. Lin, A. R. Li, X. T. Wang, B. Li, and L. Guo, Temperature-induced stacking to create Cu_2O Concave sphere for light trapping capable of ultrasensitive single-particle surface-enhanced Raman scattering, *Adv. Funct. Mater.* 28(33), 1801868 (2018)
72. W. W. Li, L. Xiong, N. C. Li, S. Pang, G. L. Xu, C. H. Yi, Z. X. Wang, G. Q. Gu, K. W. Li, W. M. Li, L. Wei, G. Y. Li, C. L. Yang, and M. Chen, Tunable 3D light trapping architectures based on self-assembled $SnSe_2$ nanoplate arrays for ultrasensitive SERS detection, *J. Mater. Chem. C* 7(33), 10179 (2019)
73. L. Shi, T. U. Tuzer, R. Fenollosa, and F. Meseguer, A new Dielectric metamaterial building block with a strong magnetic response in the sub-1.5-micrometer region: Silicon colloid nanocavities, *Adv. Mater.* 24(44), 5934 (2012)
74. P. A. Dmitriev, D. G. Baranov, V. A. Milichko, S. V. Makarov, I. S. Mukhin, A. K. Samusev, A. E. Krasnok, P. A. Belov, and Y. S. Kivshar, Resonant Raman scattering from silicon nanoparticles enhanced by magnetic response, *Nanoscale* 8(18), 9721 (2016)

75. B. J. Messinger, K. U. Raben, R. K. Chang, and P. W. Barber, Local fields at the surface of noble-metal microspheres, *Phys. Rev. B* 24(2), 649 (1981)
76. S. M. Scholz, R. Vacassy, J. Dutta, H. Hofmann, and M. Akinc, Mie scattering effects from monodispersed ZnS nanospheres, *J. Appl. Phys.* 83(12), 7860 (1998)
77. W. Ji, L. F. Li, W. Song, X. N. Wang, B. Zhao, and Y. Ozaki, Enhanced Raman scattering by ZnO superstructures: Synergistic effect of charge-transfer and Mie resonances, *Angew. Chem. Int. Ed.* 58(41), 14452 (2019)
78. S. Hayashi, R. Koh, Y. Ichiyama, and K. Yamamoto, Evidence for surface-enhanced Raman scattering on nonmetallic surfaces: Copper phthalocyanine molecules on GaP small particles, *Phys. Rev. Lett.* 60(11), 1085 (1988)
79. I. Alessandri, Enhancing Raman scattering without plasmons: Unprecedented sensitivity achieved by TiO_2 shell-based resonators, *J. Am. Chem. Soc.* 135(15), 5541 (2013)
80. N. Bontempi, I. Vassalini, S. Danesi, and I. Alessandri, ZORRO: Zirconium oxide resonators for all-in-one Raman and whispering-gallery-mode optical sensing, *Chem. Commun.* 53(75), 10382 (2017)
81. I. Rodriguez, L. Shi, X. Lu, B. A. Korgel, R. A. Alvarez-Puebla, and F. Meseguer, Silicon nanoparticles as Raman scattering enhancers, *Nanoscale* 6(11), 5666 (2014)
82. P. K. A. Campion and P. Kambhampati, Surface-enhanced Raman scattering, *Chem. Soc. Rev.* 27(4), 241 (1998)
83. L. Jensen, C. M. Aikens, and G. C. Schatz, Electronic structure methods for studying surface-enhanced Raman scattering, *Chem. Soc. Rev.* 37(5), 1061 (2008)
84. H. A. Kramers and W. Heisenberg, Über die streuung von strahlung durch atome, *Z. Phys.* 31(1), 681 (1925)
85. P. A. M. Dirac, The quantum theory of the emission and absorption of radiation, *Proc. R. Soc. Lond. A* 114(767), 243 (1927)
86. Y. S. Yamamoto and T. Itoh, Why and how do the shapes of surface enhanced Raman scattering spectra change? Recent progress from mechanistic studies, *J. Raman Spectrosc.* 47(1), 78 (2016)
87. J. I. Gersten, R. L. Birke, and J. R. Lombardi, Theory of enhance i light scattering from molecules adsorbed at the metal-solution interface, *Phys. Rev. Lett.* 43(2), 147 (1979)
88. E. Burstein, Y. J. Chen, C. Y. Chen, S. Lundquist, and E. Tosatti, "Giant" Raman scattering by adsorbed molecules on metal surfaces, *Solid State Commun.* 29(8), 567 (1979)
89. J. E. Demuth and P. N. Sanda, Observation of charge-transfer states for pyridine chemisorbed on Ag(111), *Phys. Rev. Lett.* 47(1), 57 (1981)
90. H. Yamada and Y. Yamamoto, Surface enhanced Raman scattering (SERS) of chemisorbed species on various kinds of metals and semiconductors, *Surf. Sci.* 134(1), 71 (1983)
91. H. Yamada, Y. Yamamoto, and N. Tani, Surface-enhanced Raman scattering (SERS) of adsorbed molecules on smooth surfaces of metals and a metal oxide, *Chem. Phys. Lett.* 86(4), 397 (1982)
92. A. C. Albrecht, On the theory of Raman intensities, *J. Chem. Phys.* 34(5), 1476 (1961)
93. J. R. Lombardi and R. L. Birke, Theory of surface-enhanced Raman scattering in semiconductors, *J. Phys. Chem. C* 118(20), 11120 (2014)
94. J. R. Lombardi, The theory of surface-enhanced Raman scattering on semiconductor nanoparticles: Toward the optimization of SERS sensors, *Faraday Discuss.* 205, 105 (2017)
95. S. K. Islam, M. A. Sohel, and J. R. Lombardi, Coupled exciton and charge-transfer resonances in the Raman enhancement of phonon modes of CdSe quantum dots (QDs), *J. Phys. Chem. C* 118(33), 19415 (2014)
96. X. Y. Hou, X. Y. Zhang, Q. W. Ma, X. Tang, Q. Hao, Y. C. Cheng, and T. Qiu, Alloy engineering in few-layer manganese phosphorus trichalcogenides for surface-enhanced Raman scattering, *Adv. Funct. Mater.* 30(12), 1910171 (2020)
97. X. L. Wu, Y. F. Mei, G. G. Siu, K. L. Wong, K. Moulding, M. J. Stokes, C. L. Fu, and X. M. Bao, Spherical growth and surface-quasifree vibrations of Si nanocrystallites in Er-doped Si nanostructures, *Phys. Rev. Lett.* 86(14), 3000 (2001)
98. X. L. Wu, S. J. Xiong, G. G. Siu, G. S. Huang, Y. F. Mei, Z. Y. Zhang, S. S. Deng, and C. Tan, Optical emission from excess Si defect centers in Si nanostructures, *Phys. Rev. Lett.* 91(15), 157402 (2003)
99. J. Y. Fan, X. L. Wu, and T. Qiu, Experimental evidence for quantum confinement in 3C-SiC nanoparticles, *Physics* 34(8), 570 (2005)
100. J. Wang, S. J. Xiong, X. L. Wu, T. H. Li, and P. K. Chu, Glycerol-bonded 3C-SiC nanocrystal solid films exhibiting broad and stable violet to blue-green emission, *Nano Lett.* 10(4), 1466 (2010)
101. Q. T. Liu, D. Y. Liu, J. M. Li, and Y. B. Kuang, The impact of crystal defects towards oxide semiconductor photoanode for photoelectrochemical water splitting, *Front. Phys.* 14(5), 53403 (2019)
102. H. Wu, H. Wang, and G. H. Li, Metal oxide semiconductor SERS-active substrates by defect engineering, *Analyst (Lond.)* 142(2), 326 (2017)
103. L. L. Yang, Y. S. Peng, Y. Yang, J. J. Liu, Z. Y. Li, Y. F. Ma, Z. Zhang, Y. Q. Wei, S. Li, Z. R. Huang, and N. V. Long, Green and sensitive flexible semiconductor SERS substrates: Hydrogenated black TiO_2 nanowires, *ACS Appl. Nano Mater.* 1(9), 4516 (2018)
104. P. Dharmalingam, K. Venkatakrishnan, and B. Tan, An atomic-defect enhanced Raman scattering (DERS) quantum probe for molecular level detection-breaking the SERS barrier, *Appl. Mater. Today* 16, 28 (2019)
105. X. Y. Hou, X. C. Fan, P. H. Wei, and T. Qiu, Planar transition metal oxides SERS chips: A general strategy, *J. Mater. Chem. C* 7(36), 11134 (2019)
106. X. X. Xue, W. Ji, Z. Mao, Z. S. Li, W. D. Ruan, B. Zhao, and J. R. Lombardi, Effects of Mn doping on surface enhanced Raman scattering properties of TiO_2 nanoparticles, *Spectrochim. Acta A* 95, 213 (2012)

107. P. Zuo, L. Jiang, X. Li, P. Ran, B. Li, A. S. Song, M. Y. Tian, T. B. Ma, B. S. Guo, L. T. Qu, and Y. F. Lu, Enhancing charge transfer with foreign molecules through femtosecond laser induced MoS_2 defect sites for photoluminescence control and SERS enhancement, *Nanoscale* 11(2), 485 (2019)

108. X. X. Xue, S. F. Mi, C. M. Zhao, and L. M. Chang, Investigation of surface-enhanced Raman scattering property of Ni doping ZnS nanocrystals, *J. Nanosci. Nanotechnol.* 19(12), 7748 (2019)

109. L. B. Yang, Y. Zhang, W. D. Ruan, B. Zhao, W. Q. Xu, and J. R. Lombardi, Improved surface-enhanced Raman scattering properties of TiO_2 nanoparticles by Zn dopant, *J. Raman Spectrosc.* 41(7), 721 (2009)

110. X. D. Zheng, F. Ren, S. P. Zhang, X. L. Zhang, H. Y. Wu, X. G. Zhang, Z. Xing, W. J. Qin, Y. Liu, and C. Z. Jiang, A general method for large-scale fabrication of semiconducting oxides with high SERS sensitivity, *ACS Appl. Mater. Interfaces* 9(16), 14534 (2017)

111. S. Cong, Z. Wang, W. B. Gong, Z. G. Chen, W. B. Lu, J. R. Lombardi, and Z. G. Zhao, Electrochromic semiconductors as colorimetric SERS substrates with high reproducibility and renewability, *Nat. Commun.* 10(1), 678 (2019)

112. Y. R. Liu, Z. B. Gao, M. Chen, Y. Tian, and F. Chen, Enhanced Raman scattering of CuPc films on imperfect WSe_2 monolayer correlated to exciton and charge-transfer resonances, *Adv. Funct. Mater.* 28(52), 1805710 (2018)

113. X. Y. Wang, J. Li, Y. H. Shen, and A. J. Xie, An assembled ordered $W_{18}O_{49}$ nanowire film with high SERS sensitivity and stability for the detection of RB, *Appl. Surf. Sci.* 504, 144073 (2020)

114. N. Singh, J. Prakash, M. Misra, A. Sharma, and R. K. Gupta, Dual functional Ta-doped electrospun TiO_2 nanofibers with enhanced photocatalysis and SERS detection for organic compounds, *ACS Appl. Mater. Interfaces* 9(34), 28495 (2017)

115. X. H. Li, Y. Wu, Y. H. Shen, Y. Sun, Y. Yang, and A. J. Xie, A novel bifunctional Ni-doped TiO_2 inverse opal with enhanced SERS performance and excellent photocatalytic activity, *Appl. Surf. Sci.* 427, 739 (2018)

116. X. X. Xue, W. Ji, Z. Mao, Z. S. Li, Z. N. Guo, B. Zhao, and C. Zhao, SERS study of Co-doped TiO_2 nanoparticles, *Chem. Res. Chin. Univ.* 29(4), 751 (2013)

117. L. B. Yang, X. Y. Qin, M. D. Gong, X. Jiang, M. Yang, X. L. Li, and G. Z. Li, Improving surface-enhanced Raman scattering properties of TiO_2 nanoparticles by metal Co doping, *Spectrochim. Acta A* 123, 224 (2014)

118. V. Kiran and S. Sampath, Enhanced Raman spectroscopy of molecules adsorbed on carbon-doped TiO_2 obtained from titanium carbide: A visible-light-assisted renewable substrate, *ACS Appl. Mater. Interfaces* 4(8), 3818 (2012)

119. H. J. Zhang, R. An, X. H. Ji, Y. H. Dong, F. Pan, C. Liu, and X. H. Lu, Effects of nitrogen doping on surface-enhanced Raman scattering (SERS) performance of bicrystalline TiO_2 nanofibres, *Chin. J. Chem. Eng.* 26(3), 642 (2018)

120. L. B. Yang, D. Yin, Y. Shen, M. Yang, X. L. Li, X. X. Han, X. Jiang, and B. Zhao, Mesoporous semiconducting TiO_2 with rich active sites as a remarkable substrate for surface-enhanced Raman scattering, *Phys. Chem. Chem. Phys.* 19(28), 18731 (2017)

121. R. Prabhu B, K. Bramhaiah, K. K. Singh, and N. S. John, Single sea urchin-MoO_3 nanostructure for surface enhanced Raman spectroscopy of dyes, *Nanoscale Adv.* 1(6), 2426 (2019)

122. J. Pan, M. Li, Y. Y. Luo, H. Wu, L. Zhong, Q. Wang, and G. H. Li, Synthesis and SERS activity of V_2O_5 nanoparticles, *Appl. Surf. Sci.* 333, 34 (2015)

123. M. Gao, J. C. Yao, Y. N. Quan, J. H. Yang, P. W. Huo, J. D. Dai, Y. S. Yan, and C. C. Ma, Neodymium doped zinc oxide for ultersensitive SERS substrate, *J. Mater. Sci. Mater. Electron.* 30(23), 20537 (2019)

124. S. Yang, J. C. Yao, Y. N. Quan, M. Y. Hu, R. Su, M. Gao, D. L. Han, and J. H. Yang, Monitoring the charge-transfer process in a Nd-doped semiconductor based on photoluminescence and SERS technology, *Light Sci. Appl.* 9(1), 117 (2020)

125. P. Li, X. L. Wang, X. L. Zhang, L. X. Zhang, X. W. Yang, and B. Zhao, Investigation of the charge-transfer between Ga-doped ZnO nanoparticles and molecules using surface-enhanced Raman scattering: Doping induced band-gap shrinkage, *Front. Chem.* 7, 144 (2019)

126. X. X. Xue, J. Zhang, L. Chen, C. M. Zhao, L. Wang, and L. M. Chang, Preparation and characterization of $Zn_{1-x}Ni_xO$ nanoparticles: Application as a SERS substrate, *J. Nanosci. Nanotechnol.* 18(6), 4403 (2018)

127. X. X. Xue, W. D. Ruan, L. B. Yang, W. Ji, Y. F. Xie, L. Chen, W. Song, B. Zhao, and J. R. Lombardi, Surface-enhanced Raman scattering of molecules adsorbed on Co-doped ZnO nanoparticles, *J. Raman Spectrosc.* 43(1), 61 (2012)

128. L. M. Chang, D. D. Xu, and X. X. Xue, Photoluminescence and Raman scattering study in ZnO:Mg nanocrystals, *J. Mater. Sci. Mater. Electron.* 27(1), 1014 (2016)

129. R. Haldavnekar, K. Venkatakrishnan, and B. Tan, Non plasmonic semiconductor quantum SERS probe as a pathway for in vitro cancer detection, *Nat. Commun.* 9(1), 3065 (2018)

130. J. Lin, J. Yu, O. U. Akakuru, X. T. Wang, B. Yuan, T. X. Chen, L. Guo, and A. G. Wu, Low temperature-boosted high efficiency photo-induced charge transfer for remarkable SERS activity of ZnO nanosheets, *Chem. Sci. (Camb.)* 11(35), 9414 (2020)

131. C. S. Liu, B. H. Li, C. H. Chen, J. W. Peng, and S. Lee, Enhancement in SERS intensities of azo dyes adsorbed on ZnO by plasma treatment, *J. Raman Spectrosc.* 45(5), 332 (2014)

132. J. L. Hou, X. F. Jia, X. X. Xue, L. Chen, W. Song, W. Q. Xu, and B. Zhao, Surface-enhanced Raman scattering of molecules adsorbed on SnO_2 nanoparticles, *Chem. J. Chin. Univ.* 33(1), 139 (2012)

133. X. Y. Zhou, D. Wu, Z. Jin, X. J. Song, X. F. Wang, and S. L. Suib, Significantly increased Raman enhancement on defect-rich O-incorporated 1T-MoS_2 nanosheets, *J. Mater. Sci.* 55(34), 16374 (2020)

134. X. Y. Hou, Q. Lin, Y. J. Wei, Q. Hao, Z. H. Ni, and T. Qiu, Surface-enhanced Raman scattering monitoring of oxidation states in defect-engineered two-dimensional transition metal dichalcogenides, *J. Phys. Chem. Lett.* 11(19), 7981 (2020)

135. M. L. Chen, K. Li, Y. Y. Luo, J. P. Shi, C. C. Weng, L. Gao, and G. T. Duan, Improved SERS activity of non-stoichiometric copper sulfide nanostructures related to charge-transfer resonance, *Phys. Chem. Chem. Phys.* 22(9), 5145 (2020)

136. P. Ji, Z. Mao, Z. Wang, X. X. Xue, Y. Zhang, J. Lv, and X. M. Shi, Improved surface-enhanced Raman scattering properties of ZrO_2 nanoparticles by Zn doping, *Nanomaterials (Basel)* 9(7), 983 (2019)

137. Y. M. Yang, T. Qiu, F. Kong, J. Y. Fan, H. L. Ou, Q. Y. Xu, and P. K. Chu, Interference effects on indium tin oxide enhanced Raman scattering, *J. Appl. Phys.* 111(3), 033110 (2012)

138. Y. M. Yang, K. L. Long, F. Kong, J. Y. Fan, and T. Qiu, Surface-enhanced Raman spectroscopy on transparent fume-etched ITO-glass surface, *Appl. Surf. Sci.* 309, 250 (2014)

139. L. Hu, Z. Xu, F. Long, J. Yuan, H. Li, A. Zhao, S. Han, N. Zhang, X. Liu, C. Ma, S. Ruan, and Y. Zeng, Direct bandgap opening in sodium-doped antimonene quantum dots: An emerging 2D semiconductor, *Mater. Horiz.* 7(6), 1588 (2020)

140. G. T. Wang, H. N. Wei, Y. Tian, M. M. Wu, Q. Q. Sun, Z. S. Peng, L. F. Sun, and M. Liu, Twin-ZnSe nanowires as surface enhanced Raman scattering substrate with significant enhancement factor upon defect, *Opt. Express* 28(13), 18843 (2020)

141. I. C. Y. Chang, Y. S. Sun, Y. W. Yang, C. H. Wang, S. L. Cheng, and W. W. Hu, Effects of graphitization and bonding configuration in iron-nitrogen-doped carbon nanostructures on surface-enhanced Raman scattering, *ACS Appl. Nano Mater.* 3(1), 858 (2020)

142. Y. Gao, N. Gao, H. D. Li, X. X. Yuan, Q. L. Wang, S. H. Cheng, and J. S. Liu, Semiconductor SERS of diamond, *Nanoscale* 10(33), 15788 (2018)

143. S. S. Wen, X. W. Ma, H. Liu, G. Chen, H. Wang, G. Q. Deng, Y. T. Zhang, W. Song, B. Zhao, and Y. Ozaki, Accurate monitoring platform for the surface catalysis of nanozyme validated by surface-enhanced Raman-kinetics model, *Anal. Chem.* 92(17), 11763 (2020)

144. Y. Tian, H. N. Wei, Y. J. Xu, Q. Q. Sun, B. Y. Man, and M. Liu, Influence of SERS activity of $SnSe_2$ nanosheets doped with sulfur, *Nanomaterials (Basel)* 10(10), 1910 (2020)

145. J. E. Medvedeva, D. B. Buchholz, and R. P. H. Chang, Recent Advances in understanding the structure and properties of amorphous oxide semiconductors, *Adv. Electron. Mater.* 3(9), 1700082 (2017)

146. A. R. Li, J. Lin, Z. N. Huang, X. T. Wang, and L. Guo, Surface-enhanced Raman spectroscopy on amorphous semiconducting rhodium sulfide microbowl substrates, *iScience* 10, 1 (2018)

147. A. R. Li, J. Yu, J. Lin, M. Chen, X. T. Wang, L. Guo, and O. Increased, Increased O 2p state density enabling significant photoinduced charge transfer for surface-enhanced Raman scattering of amorphous $Zn(OH)_2$, *J. Phys. Chem. Lett.* 11(5), 1859 (2020)

148. M. S. Gao, P. Miao, X. J. Han, C. Sun, Y. Ma, Y. L. Gao, and P. Xu, Hollow transition metal hydroxide octahedral microcages for single particle surface-enhanced Raman spectroscopy, *Inorg. Chem. Front.* 6(9), 2318 (2019)

149. L. L. Yang, Y. Q. Wei, Y. S. Song, Y. S. Peng, Y. Yang, and Z. R. Huang, Surface-enhanced Raman scattering from amorphous nanoflower-structural Nb_2O_5 fabricated by two-step hydrothermal technology, *Mater. Des.* 193, 108808 (2020)

150. E. Er, H. L. Hou, A. Criado, J. Langer, M. Moller, N. Erk, L. M. Liz-Marzan, and M. Prato, High-yield preparation of exfoliated 1T-MoS_2 with SERS activity, *Chem. Mater.* 31(15), 5725 (2019)

151. C. L. Tan, Z. M. Luo, A. Chaturvedi, Y. Q. Cai, Y. H. Du, Y. Gong, Y. Huang, Z. C. Lai, X. Zhang, L. R. Zheng, X. Y. Qi, M. H. Goh, J. Wang, S. K. Han, X. J. Wu, L. Gu, C. Kloc, and H. Zhang, Preparation of high-percentage 1T-phase transition metal dichalcogenide nanodots for electrochemical hydrogen evolution, *Adv. Mater.* 30(9), 1705509 (2018)

152. T. A. Empante, Y. Zhou, V. Klee, A. E. Nguyen, I. Lu, M. D. Valentin, S. A. Naghibi Alvillar, E. Preciado, A. J. Berges, C. S. Merida, M. Gomez, S. Bobek, M. Isarraraz, E. J. Reed, and L. Bartels, Chemical vapor deposition growth of few-layer $MoTe_2$ in the 2H, 1T , and 1T phases: Tunable properties of $MoTe_2$ films, *ACS Nano* 11(1), 900 (2017)

153. P. Miao, J. Wu, Y. C. Du, Y. C. Sun, and P. Xu, Phase transition induced Raman enhancement on vanadium dioxide (VO_2) nanosheets, *J. Mater. Chem. C* 6(40), 10855 (2018)

154. D. R. Miller, S. A. Akbar, and P. A. Morris, Nanoscale metal oxide-based heterojunctions for gas sensing: A review, *Sens. Actuators B Chem.* 204, 250 (2014)

155. T. Q. Niu, J. Lu, X. G. Jia, Z. Xu, M. C. Tang, D. Barrit, N. Y. Yuan, J. N. Ding, X. Zhang, Y. Y. Fan, T. Luo, Y. L. Zhang, D. Smilgies, Z. K. Liu, A. Amassian, S. Y. Jin, K. Zhao, and S. Z. Liu, Interfacial engineering at the 2D/3D heterojunction for high-performance perovskite solar cells, *Nano Lett.* 19(10), 7181 (2019)

156. S. A. Ghopry, M. A. Alamri, R. Goul, R. Sakidja, and J. Z. Wu, Extraordinary sensitivity of surface-enhanced Raman spectroscopy of molecules on MoS_2 (WS_2) nanodomes/graphene van der Waals heterostructure substrates, *Adv. Opt. Mater.* 7(8), 1801249 (2019)

157. Q. Cai, W. Gan, A. Falin, K. Watanabe, T. Taniguchi, J. C. Zhuang, W. C. Hao, S. M. Huang, T. Tao, Y. Chen, and L. H. Li, Two-dimensional van der Waals heterostructures for synergistically improved surface-enhanced Raman spectroscopy, *ACS Appl. Mater. Interfaces* 12(19), 21985 (2020)

158. H. Kitadai, X. Z. Wang, N. N. Mao, S. X. Huang, and X. Ling, Enhanced Raman scattering on nine 2D van der Waals materials, *J. Phys. Chem. Lett.* 10(11), 3043 (2019)

159. J. Lin, W. Z. Ren, A. R. Li, C. Y. Yao, T. X. Chen, X. H. Ma, X. T. Wang, and A. G. Wu, Crystal-amorphous core-shell structure synergistically enabling TiO_2 nanoparticles' remarkable SERS sensitivity for cancer cell imaging, *ACS Appl. Mater. Interfaces* 12(4), 4204 (2020)

160. K. N. Zhang, Y. Zhang, T. N. Zhang, W. J. Dong, T. X. Wei, Y. Sun, X. Chen, G. Z. Zhen, and N. Dai, Vertically coupling ZnO nanorods on MoS_2 monolayers with enhanced Raman and photoluminescence emission, *Nano Res.* 8(3), 743 (2015)

161. L. G. Quagliano, Observation of molecules adsorbed on III-V semiconductor quantum dots by surface-enhanced Raman scattering, *J. Am. Chem. Soc.* 126(23), 7393 (2004)

162. M. Dandu, K. Watanabe, T. Taniguchi, A. K. Sood, and K. Majumdar, Spectrally tunable, large Raman enhancement from nonradiative energy transfer in the van der Waals heterostructure, *ACS Photon.* 7(2), 519 (2020)

163. M. P. Chen, B. Ji, Z. Y. Dai, X. Y. Du, B. C. He, G. Chen, D. Liu, S. Chen, K. H. Lo, S. P. Wang, B. P. Zhou, and H. Pan, Vertically-aligned 1T/2H-MS_2 (M = Mo, W) nanosheets for surface-enhanced Raman scattering with long-term stability and large-scale uniformity, *Appl. Surf. Sci.* 527, 146769 (2020)

164. S. G. Pan, X. H. Liu, and X. Wang, Preparation of Ag_2S-graphene nanocomposite from a single source precursor and its surface-enhanced Raman scattering and photoluminescent activity, *Mater. Charact.* 62(11), 1094 (2011)

165. J. L. Lopes, S. Fateixa, A. C. Estrada, J. D. Gouveia, J. R. B. Gomes, and T. Trindade, Surface-enhanced Raman scattering due to a synergistic effect on ZnS and graphene oxide, *J. Phys. Chem. C* 124(23), 12742 (2020)

166. I. Alessandri, and L. E. Depero, All-oxide Raman-active traps for light and matter: Probing redox homeostasis model reactions in aqueous environment, *Small* 10(7), 1294 (2014)

167. D. Papadakis, A. Diamantopoulou, P. A. Pantazopoulos, D. Palles, E. Sakellis, N. Boukos, N. Stefanou, and V. Likodimos, Nanographene oxide-TiO_2 photonic films as plasmon-free substrates for surface-enhanced Raman scattering, *Nanoscale* 11(44), 21542 (2019)

168. T. T. Zheng, E. D. Feng, Z. Q. Wang, X. Q. Gong, and Y. Tian, Mechanism of surface-enhanced Raman scattering based on 3D graphene-TiO_2 nanocomposites and application to real-time monitoring of telomerase activity in differentiation of stem cells, *ACS Appl. Mater. Interfaces* 9(42), 36596 (2017)

169. R. C. Wang, Y. H. Chen, H. H. Huang, K. T. Lin, Y. S. Jheng, and C. Y. Liu, Justification of dipole mechanism over chemical charge transfer mechanism for dipole-based SERS platform with excellent chemical sensing performance, *Appl. Surf. Sci.* 521, 146426 (2020)

170. B. C. Qiu, M. Y. Xing, Q. Y. Yi, and J. L. Zhang, Chiral carbonaceous nanotubes modified with titania nanocrystals: plasmon-free and recyclable SERS sensitivity, *Angew. Chem. Int. Ed.* 54(36), 10643 (2015)

171. X. Jiang, D. Yin, M. Yang, J. Du, W. E. Wang, L. Zhang, L. B. Yang, X. X. Han, and B. Zhao, Revealing interfacial charge transfer in TiO_2/reduced graphene oxide nanocomposite by surface-enhanced Raman scattering (SERS): Simultaneous a superior SERS-active substrate, *Appl. Surf. Sci.* 487, 938 (2019)

172. X. Jiang, Q. Q. Sang, M. Yang, J. Du, W. E. Wang, L. B. Yang, X. X. Han, and B. Zhao, Metal-free SERS substrate based on rGO-TiO_2-Fe_3O_4nnanohybrid: Contribution from interfacial charge transfer and magnetic controllability, *Phys. Chem. Chem. Phys.* 21(24), 12850 (2019)

173. E. D. Feng, T. T. Zheng, X. X. He, J. Q. Chen, and Y. Tian, A novel ternary heterostructure with dramatic SERS activity for evaluation of PD-L1 expression at the single-cell level, *Sci. Adv.* 4(11), eaau3494 (2018)

174. D. Yin, M. L. Wang, Y. Z. Wang, X. Hu, B. Liu, H. Liu, L. L. Ma, and G. G. Gao, A ternary ZnO/ZnS/MoS_2 composite as a reusable SERS substrate derived from the polyoxomolybdate/ZIF-8 host–guest framework, *J. Mater. Chem. C* 7(32), 9856 (2019)

175. Y. N. Quan, J. C. Yao, Y. S. Sun, X. Qu, R. Su, M. Y. Hu, L. Chen, Y. Liu, M. Gao, and J. H. Yang, Enhanced semiconductor charge-transfer resonance: Unprecedented oxygen bidirectional strategy, *Sens. Actuators B Chem.* 327, 128903 (2021)

176. Y. N. Quan, J. C. Yao, S. Yang, L. Chen, J. Li, Y. Liu, J. Lang, H. Shen, Y. Wang, Y. Wang, J. Yang, and M. Gao, ZnO nanoparticles on MoS_2 microflowers for ultrasensitive SERS detection of bisphenol A, *Mikrochim. Acta* 186(8), 593 (2019)

177. H. W. Qiu, M. Q. Wang, L. Zhang, M. H. Cao, Y. Q. Ji, S. Kou, J. J. Dou, X. Q. Sun, and Z. Yang, Wrinkled 2H-phase MoS_2 sheet decorated with graphene-microflowers for ultrasensitive molecular sensing by plasmon-free SERS enhancement, *Sens. Actuators B Chem.* 320, 128445 (2020)

178. M. Y. Xin, Y. Z. Fu, Y. Zhou, J. H. Han, Y. L. Mao, M. J. Li, J. H. Liu, and M. J. Huang, The surface-enhanced Raman scattering of all-inorganic perovskite quantum dots of $CsPbBr_3$ encapsulated in a ZIF-8 metal-organic framework, *New J. Chem.* 44(40), 17570 (2020)

179. G. Liu, J. C. Yu, G. Q. Lu, and H. M. Cheng, Crystal facet engineering of semiconductor photocatalysts: Motivations, advances and unique properties, *Chem. Commun. (Camb.)* 47(24), 6763 (2011)

180. X. Gao and T. Zhang, An overview: Facet-dependent metal oxide semiconductor gas sensors, *Sens. Actuators B Chem.* 277, 604 (2018)

181. F. Wang, X. Wang, Z. Chang, Y. Zhu, L. Fu, X. Liu, and Y. Wu, Electrode materials with tailored facets for electrochemical energy storage, *Nanoscale Horiz.* 1(4), 272 (2016)

182. I. Urdaneta, A. Keller, O. Atabek, J. L. Palma, D. Finkelstein-Shapiro, P. Tarakeshwar, V. Mujica, and M. Calatayud, Dopamine adsorption on TiO_2 anatase surfaces, *J. Phys. Chem. C* 118(35), 20688 (2014)

183. X. L. Zheng, H. L. Guo, Y. Xu, J. L. Zhang, and L. Z. Wang, Improving SERS sensitivity of TiO_2 by utilizing the heterogeneity of facet-potentials, *J. Mater. Chem. C* 8(39), 13836 (2020)

184. J. L. Wang, F. Xiao, J. Yan, Z. Wu, K. K. Liu, Z. F. Chang, R. B. Zhang, H. Chen, H. B. Wu, and Y. Cao, Difluorobenzothiadiazole-based small-molecule organic solar cells with 8.7% efficiency by tuning of -conjugated spacers and solvent vapor annealing, *Adv. Funct. Mater.* 26(11), 1803 (2016)

185. C. L. Zhou, L. F. Sun, F. Q. Zhang, C. J. Gu, S. W. Zeng, T. Jiang, X. Shen, D. S. Ang, and J. Zhou, Electrical tuning of the SERS enhancement by precise defect density control, *ACS Appl. Mater. Interfaces* 11(37), 34091 (2019)

186. P. Li, X. L. Wang, H. Y. Li, X. W. Yang, X. L. Zhang, L. X. Zhang, Y. Ozaki, B. B. Liu, and B. Zhao, Investigation of charge-transfer between a 4-mercaptobenzoic acid monolayer and TiO_2 nanoparticles under high pressure using surface-enhanced Raman scattering, *Chem. Commun. (Camb.)* 54(49), 6280 (2018)

187. H. H. Sun, M. G. Yao, Y. P. Song, L. Y. Zhu, J. J. Dong, R. Liu, P. Li, B. Zhao, and B. B. Liu, Pressure-induced SERS enhancement in a MoS_2/Au/R6G system by a two-step charge transfer process, *Nanoscale* 11(44), 21493 (2019)

188. X. H. Li, S. H. Guo, J. Su, X. G. Ren, and Z. Y. Fang, Efficient Raman enhancement in molybdenum disulfide by tuning the interlayer spacing, *ACS Appl. Mater. Interfaces* 12(25), 28474 (2020)

189. Y. Y. Qiu, M. Lin, G. X. Chen, C. C. Fan, M. W. Li, X. J. Gu, S. Cong, Z. G. Zhao, L. Fu, X. H. Fang, and Z. Y. Xiao, Photodegradable CuS SERS probes for intraoperative residual tumor detection, ablation, and self-clearance, *ACS Appl. Mater. Interfaces* 11(26), 23436 (2019)

190. J. Surmacki, Nitrogen-doped titanium dioxide nanoparticles modified by an electron beam for improving human breast cancer detection by Raman spectroscopy: A preliminary study, *Diagnostics (Basel)* 10(10), 757 (2020)

191. S. Ganesh, K. Venkatakrishnan, and B. Tan, Quantum scale organic semiconductors for SERS detection of DNA methylation and gene expression, *Nat. Commun.* 11(1), 1135 (2020)

192. R. A. Alvarez-Puebla and L. M. Liz-Marzan, SERS detection of small inorganic molecules and ions, *Angew. Chem. Int. Ed.* 51(45), 11214 (2012)

193. W. Ji, Y. Wang, I. Tanabe, X. X. Han, B. Zhao, and Y. Ozaki, Semiconductor-driven "turn-off" surface-enhanced Raman scattering spectroscopy: Application in selective determination of chromium(vi) in water, *Chem. Sci. (Camb.)* 6(1), 342 (2015)

194. B. P. Majee, S. Mishra, R. K. Pandey, R. Prakash, and A. K. Mishra, Multifunctional few-layer MoS_2 for photodetection and surface-enhanced Raman spectroscopy application with ultrasensitive and repeatable detectability, *J. Phys. Chem. C* 123(29), 18071 (2019)

195. N. Bontempi, I. Vassalini, and I. Alessandri, All-dielectric core/shell resonators: From plasmon-free SERS to multimodal analysis, *J. Raman Spectrosc.* 49(6), 943 (2018)

196. X. X. Han, C. Kohler, J. Kozuch, U. Kuhlmann, L. Paasche, A. Sivanesan, I. M. Weidinger, and P. Hildebrandt, Potential-dependent surface-enhanced resonance Raman spectroscopy at nanostructured TiO_2: A case study on cytochrome b_5, *Small* 9(24), 4175 (2013)

197. I. Alessandri and L. E. Depero, All-oxide Raman-active traps for light and matter: Probing redox homeostasis model reactions in aqueous environment, *Small* 10(7), 1294 (2014)

198. D. Glass, E. Cortes, S. Ben-Jaber, T. Brick, W. J. Peveler, C. S. Blackman, C. R. Howle, R. Quesada-Cabrera, I. P. Parkin, and S. A. Maier, Dynamics of photo-induced surface oxygen vacancies in metal-oxide semiconductors studied under ambient conditions, *Adv. Mater.* 6(22), 1901841 (2019)

199. X. Y. Zhang, S. Yang, L. L. Yang, D. X. Zhang, Y. Sun, Z. Y. Pang, J. H. Yang, and L. Chen, Carrier dynamic monitoring of a p-conjugated polymer: A surface-enhanced Raman scattering method, *Chem. Commun.* 56(18), 2779 (2020)

200. P. Tarakeshwar, J. L. Palma, D. Finkelstein-Shapiro, A. Keller, I. Urdaneta, M. Calatayud, O. Atabek, and V. Mujjica, SERS as a probe of charge-transfer pathways in hybrid dye/molecule-metal oxide complexes, *J. Phys. Chem. C* 118(7), 3774 (2014)

201. Z. H. Kim, Single-molecule surface-enhanced Raman scattering: Current status and future perspective, *Front. Phys.* 9(1), 25 (2014)

202. X. Y. Hou, X. G. Luo, X. C. Fan, Z. H. Peng, and T. Qiu, Plasmon-coupled charge transfer in WO_{3-x} semiconductor nanoarrays: toward highly uniform silver-comparable SERS platforms, *Phys. Chem. Chem. Phys.* 21(5), 2611 (2019)

203. W. Liu, H. Bai, X. S. Li, W. T. Li, J. F. Zhai, J. F. Li, and G. C. Xi, Improved surface-enhanced Raman spectroscopy sensitivity on metallic tungsten oxide by the synergistic effect of surface plasmon resonance coupling and charge transfer, *J. Phys. Chem. Lett.* 9(14), 4096 (2018)

204. J. H. Wang, Y. H. Yang, H. Li, J. Gao, P. He, L. Bian, F. Q. Dong, and Y. He, Stable and tunable plasmon resonance of molybdenum oxide nanosheets from the ultraviolet to the near-infrared region for ultrasensitive surface-enhanced Raman analysis, *Chem. Sci. (Camb.)* 10(25), 6330 (2019)

205. Z. Tian, H. Bai, C. Chen, Y. T. Ye, Q. H. Kong, Y. H. Li, W. H. Fan, W. C. Yi, and G. C. Xi, Quasi-metal for highly sensitive and stable surface-enhanced Raman scattering, *iScience* 19(27), 836 (2019)

206. X. J. Tan, L. Z. Wang, C. Cheng, X. F. Yan, B. Shen, and J. L. Zhang, Plasmonic MoO_{3-x}@MoO_3 nanosheets for highly sensitive SERS detection through nanoshell-isolated electromagnetic enhancement, *Chem. Commun. (Camb.)* 52(14), 2893 (2016)

207. Q. Q. Zhang, X. S. Li, Q. Ma, Q. Zhang, H. Bai, W. C. Yi, J. Y. Liu, J. Han, and G. C. Xi, A metallic molybdenum dioxide with high stability for surface enhanced Raman spectroscopy, *Nat. Commun.* 8(1), 14903 (2017)

208. Q. Zhu, S. L. Jiang, K. Ye, W. Hu, J. C. Zhang, X. Y. Niu, Y. X. Lin, S. M. Chen, L. Song, Q. Zhang, J. Jiang, and Y. Luo, Hydrogen-doping-induced metal-like ultrahigh free-carrier concentration in metal-oxide material for giant and tunable plasmon resonance, *Adv. Mater.* 32(50), 2004059 (2020)

209. P. Li, L. Zhu, C. Ma, L. X. Zhang, L. Guo, Y. W. Liu, H. Ma, and B. Zhao, Plasmonic molybdenum tungsten oxide hybrid with surface-enhanced Raman scattering comparable to that of noble metals, *ACS Appl. Mater. Interfaces* 12(16), 19153 (2020)

210. Y. T. Ye, W. C. Yi, W. Liu, Y. Zhou, H. Bai, J. F. Li, and G. C. Xi, Remarkable surface-enhanced Raman scattering of highly crystalline monolayer Ti_3C_2 nanosheets, *Sci. China Mater.* 63(5), 794 (2020)

211. H. M. Guan, W. C. Yi, T. Li, Y. H. Li, J. F. Li, H. Bai, and G. C. Xi, Low temperature synthesis of plasmonic molybdenum nitride nanosheets for surface enhanced Raman scattering, *Nat. Commun.* 11(1), 3889 (2020)

212. F. T. Zhao, X. T. Xue, W. Y. Fu, Y. H. Liu, Y. H. Ling, and Z. J. Zhang, TiN nanorods as effective substrate for surface-enhanced Raman scattering, *J. Phys. Chem. C* 123(48), 29353 (2019)

213. R. F. Du, W. C. Yi, W. T. Li, H. F. Yang, H. Bai, J. F. Li, and G. C. Xi, Quasi-metal microwave route to MoN and Mo_2C ultrafine nanocrystalline hollow spheres as surface-enhanced Raman scattering substrates, *ACS Nano* 14(10), 13718 (2020)

214. A. Agrawal, S. H. Cho, O. Zandi, S. Ghosh, R. W. Johns, and D. J. Milliron, Localized surface plasmon resonance in semiconductor nanocrystals, *Chem. Rev.* 118(6), 3121 (2018)

215. C. D'Andrea, J. Bochterle, A. Toma, C. Huck, F. Neubrech, E. Messina, B. Fazio, O. M. Marago, E. Di Fabrizio, M. L. de la Chapelle, P. G. Gucciardi, and A. Pucci, Optical nanoantennas for multiband surface-Enhanced infrared and Raman spectroscopy, *ACS Nano* 7(4), 3522 (2013)

216. A. Pallaoro, G. B. Braun, N. O. Reich, and M. Moskovits, Mapping local pH in live cells using encapsulated fluorescent SERS nanotags, *Small* 6(5), 618 (2010)

217. T. X. Huang, C. W. Li, L. K. Yang, J. F. Zhu, X. Yao, C. Liu, K. Q. Lin, Z. C. Zeng, S. S. Wu, X. Wang, F. Z. Yang, and B. Ren, Rational fabrication of silver-coated AFM TERS tips with a high enhancement and long lifetime, *Nanoscale* 10(9), 4398 (2018)

218. H. S. Lai, G. K. Li, F. G. Xu, and Z. M. Zhang, Metal-organic frameworks: Opportunities and challenges for surface-enhanced Raman scattering — a review, *J. Mater. Chem. C* 8(9), 2952 (2020)

219. Q. Q. Ding, J. Wang, X. Y. Chen, H. Liu, Q. J. Li, Y. L. Wang, and S. K. Yang, Quantitative and sensitive SERS platform with analyte enrichment and filtration function, *Nano Lett.* 20(10), 7304 (2020)

220. J. Z. Chen, G. G. Liu, Y. Z. Zhu, M. Su, P. F. Yin, X. J. Wu, Q. P. Lu, C. L. Tan, M. T. Zhao, Z. Q. Liu, W. M. Yang, H. Li, G. H. Nam, L. P. Zhang, Z. H. Chen, X. Huang, P. M. Radjenovic, W. Huang, Z. Q. Tian, J. F. Li, and H. Zhang, Ag@MoS_2 core-shell heterostructure as SERS platform to reveal the hydrogen evolution active sites of single-layer MoS_2, *J. Am. Chem. Soc.* 142(15), 7161 (2020)

221. X. Zhao, J. Dong, E. Cao, Q. Y. Han, W. Gao, Y. K. Wang, J. X. Qi, and M. T. Sun, Plasmon-exciton coupling by hybrids between graphene and gold nanorods vertical array for sensor, *Appl. Mater. Today* 14, 166 (2019)

222. H. K. Lee, Y. H. Lee, C. S. L. Koh, G. C. Phan-Quang, X. Han, C. L. Lay, H. Y. F. Sim, Y. C. Kao, Q. An, and X. Y. Ling, Designing surface-enhanced Raman scattering (SERS) platforms beyond hotspot engineering: Emerging opportunities in analyte manipulations and hybrid materials, *Chem. Soc. Rev.* 48(3), 731 (2019)

223. X. Z. Qiao, B. S. Su, C. Liu, Q. Song, D. Luo, G. Mo, and T. Wang, Selective surface enhanced Raman scattering for quantitative detection of lung cancer biomarkers in superparticle@MOF structure, *Adv. Mater.* 30(5), 1702275 (2018)